CHEMICAL REVIEWS

Review

Cite This: *Chem. Rev.* XXXX, XXX, XXX−XXX

pubs.acs.org/CR

Force Generation by Myosin Motors: A Structural Perspective

Julien Robert-Paganin,[†] Olena Pylypenko,[†] Carlos Kikuti,[†] H. Lee Sweeney,[‡] and Anne Houdusse*[,†]

[†]Structural Motility, UMR 144 CNRS/Curie Institute, 26 rue d'ulm, 75258 Paris cedex 05, France

[‡]Department of Pharmacology & Therapeutics and the Myology Institute, University of Florida College of Medicine, PO Box 100267, Gainesville, Florida 32610-0267, United States

ABSTRACT: Generating force and movement is essential for the functions of cells and organisms. A variety of molecular motors that can move on tracks within cells have evolved to serve this role. How these motors interact with their tracks and how that, in turn, leads to the generation of force and movement is key to understanding the cellular roles that these motor-track systems serve. This review is focused on the best understood of these systems, which is the molecular motor myosin that moves on tracks of filamentous (F-) actin. The review highlights both the progress and the limits of our current understanding of how force generation can be controlled by F-actin−myosin interactions. What has emerged are insights they may serve as a framework for understanding the design principles of a number of types of molecular motors and their interactions with their tracks.

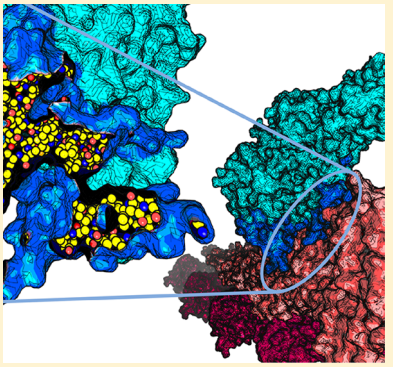

CONTENTS

Special Issue: Molecular Motors

Received: April 29, 2019

DOI: 10.1021/acs.chemrev.9b00264
Chem. Rev. XXXX, XXX, XXX−XXX

1. INTRODUCTION—IMPORTANCE OF MYOSIN FORCE GENERATION IN LIVING CELLS

Producing directed motions in cells requires a combination of polarized polymeric tracks and nanomachines (molecular motors) that can move or exert forces along those tracks. The forces and movements generated by the molecular motors interacting with their tracks are powered by harnessing the free energy of the ATP disequilibrium. For this chemo-mechanical transduction to be productive, it requires gating (to ensure that only productive interactions are maintained) and rectification that is provided by stereospecific motor−track interactions. The first biological track and motor system to be described was the actin−myosin system that powers muscle contraction, wherein filaments made of actin are the track and myosin is the motor. Later, it was discovered that the actin−myosin system encompasses many classes of specialized myosin motors that can move on actin tracks to power a large number of processes in cells. Of all of the molecular motor and track interactions that exist in cells, the mechanism of chemo-mechanical transduction is best understood for the actin−myosin interaction. This review will focus on what is understood about this mechanism, the questions that remain unanswered, and the applicability of these design principles to how molecular motors in general function in cells.

1.1. Importance of Actin-Based Molecular Motors in Health and Disease

Many cellular functions require directed movements and the generation of forces that are achieved by molecular motors moving on polarized tracks consisting of microtubules, actin filaments, DNA, or RNA. The actin−myosin system powers not only the contraction of muscle but also such functions as cytokinesis, cells crawling on surfaces, formation of diverse forms of cellular protrusions, and aspects of endo- and exocytosis as well as Golgi function.[1−4] While actin and the corresponding actin filaments are highly conserved, the myosin motors that move upon them are much more divergent. Twelve distinct classes of myosins are expressed in mammals,[4] and each class is specialized for different types of cellular functions.

The basic myosin blueprint is conserved among the different classes (Figure 1a). The **motor domain** (containing the actin binding interface as well as the active site that binds and hydrolyzes ATP) is followed by the **lever arm**, which is an elongated region of variable length among myosins that extends from the motor domain. The main role of the lever arm is to amplify the conformational changes that occur in the motor domain during force production. The **tail** region is also of variable length and structural composition and plays a critical role in specific recruitment and assembly of motors. Depending on the myosin class, it can be composed of a diverse globular domain called the **Cargo Binding domain** (**CBD**) and may also contain motifs (such as coiled-coil regions) that promote assembly of motors.

There are a number of critical design features that allow different classes of myosins to carry out their individual cellular roles. The most obvious is the inclusion of specialized regions that are designed to interact with specific proteins (i.e., cargoes) and either move and/or exert forces upon them.[5] Motor/track interactions are required for force production, and a number of class-specific forms of regulation have evolved to prevent the interaction of myosin with actin until force generation and movement is required to meet a functional demand.[6] Inactive forms of the motors in cells are disrupted by cargo recognition or signaling,[6−8] which thus specifies where in the cells the myosins will perform their functions. The actin tracks are polarized, dictating the direction of movement of the myosin motors. With the exception of only one known class of myosins (class VI or Myo6),[7,9] myosin motors move toward the + or fast-growing end of actin filaments.

Myosins are molecular motors that produce force in an ATP-dependent manner. The hydrolysis state of the nucleotide governs the affinity of the motor for the track as well as the conformational changes within the motor domain that lead to the lever arm swing (Figure 1b). Also of critical importance is the fraction of the ATPase cycle that the motors remain bound to actin (known as the **duty ratio**), both in the absence and presence of load on the motor. This can allow a single, two-headed, high-duty-ratio myosin to move a cargo for long runs (processive movement) or stall it on an actin filament under load (Figure 1c,d). Other types of myosin motors work in ensembles of low-duty-ratio myosins to exert forces as an assembly of motors while enabling rapid movements, such as what occurs in the sarcomeres of muscle (Figure 1e).[3,13,14]

Mutations in the myosin genes can lead to human disease. There are diseases associated with virtually every class of myosin.[2,15−17] The types of mutations range from missense mutations that have subtle impacts on the motor function to truncating mutations that result in complete loss of the myosin. The myosin for which the most human-disease-causing mutations are known is the beta-cardiac myosin (a class II myosin) of the heart. In this case, mutations that cause subtle changes in function cause cardiomyopathies due to the fact that the heart is such a precisely tuned pump. Loss of this myosin would obviously be lethal, but the disease rises from the fact that a single amino acid change in the sequence of the motor domain can affect the amount of force produced or change the amount of motors involved in contraction,[17,18] which is sufficient to cause cardiomyopathies.[15] Loss of other classes of myosin due to truncating mutations can be tolerated in terms of viability but can lead to various forms of disease, based on which cell types are most dependent on that class of myosin. For instance, hair cells from the inner ear, that are essential for hearing, cannot survive without class VI myosin, but other tissues are much less impacted by the loss.[19,20] Recent advances have led to identification of small molecules that can modulate structural transitions and tune the force produced by these motors.[21−27] For cardiomyopathies, drugs are currently in phase 3 clinical trials that can either enhance or decrease the force produced by cardiac myosin.

Current mechanistic models for force production are limited by our lack of knowledge about the transitions on F-actin that trigger the rearrangements in the motor that are linked to force production. How sequence differences can lead to different motor properties or how mutations can alter force production

DOI: 10.1021/acs.chemrev.9b00264
Chem. Rev. XXXX, XXX, XXX−XXX

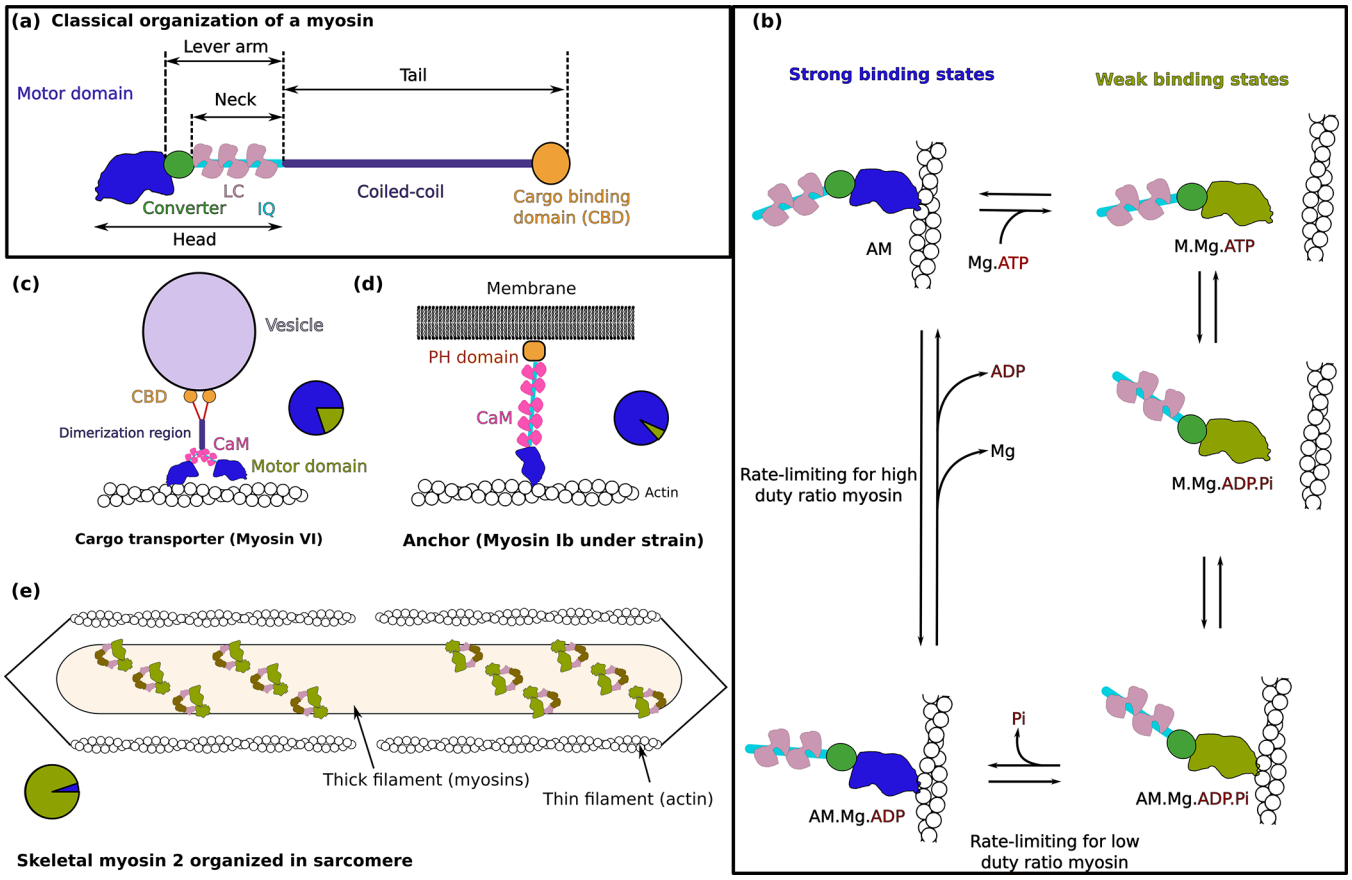

Figure 1. (a) Blueprint of a myosin. (b) Simplified representation of the ATP-dependent motor cycle of a myosin. Here the motor domains are colored depending on whether they represent weak (green) or strong (blue) binding states of the motor to actin. Depending on the rate-limiting steps within the cycle, a myosin can remain bound to actin in states of strong affinity for actin for a significant or small amount of its overall cycle (high or low duty ratio, respectively). (c–e) Examples of myosin motors with differing duty ratios. The pie chart accompanying each example represents the duty ratio by showing the ratio between weak (green) and strong (blue) binding states for actin of the overall ATPase cycle. (c) Cargo transporters, such as Myo6, are dimeric, and they are high-duty-ratio motors. (d) Myo1b functions as an anchor under strain. The motor binds lipid membranes via the tail and acts as a tension-sensitive dock or tether between the actin cytoskeleton and the membrane. (e) Organization in sarcomeres of muscle Myo2, with the heads depicted in an interacting-head motif that is found in Myo2 filaments.[10−12] These myosins are low-duty-ratio myosins.

is currently unclear. This review will summarize the most recent insights on how force is produced and modulated by structural differences in these myosin motors, which should guide the future design of myosin-based therapies for human diseases.

1.2. Brief Overview of the Actin and Myosin Structures

1.2.1. Actin: The Universal Track. Actin is an exceptionally conserved and abundant protein among the eukaryotes. It is the building block of the thin and flexible filaments of the cell cytoskeleton. Numerous proteins bind actin and regulate the lifetime and the building of F-actin assemblies in cells. Actin polymerization in networks can itself produce force. Cells generate and transmit forces across large distances to mediate cellular membrane deformation and cell motility by harnessing actin polymerization, branching, and cross-linking.[28,29] Here we will focus on the force produced by molecular motors that belong to the myosin superfamily, which all use this universal track to generate distinct and specific forces and movements in cells.

The unpolymerized monomeric protein, G-actin, is made of four subdomains,[30] with a central nucleotide binding pocket (Figure 2a) and a hydrophobic cleft between subdomains 1 and 3 that provides the majority of interactions with actin binding proteins. The breakthrough filamentous-actin (F-actin) structure was determined to 3.3 × 5.6 Å resolution from X-ray fiber diffraction by Oda et al. in 2009.[31] This structure revealed how the actin subunit within the filament differs in the position of the subdomains compared to the free G-actin monomer. Adding an actin monomer to the filament requires the flattening of its four-subunit structure[31] (Figure 2b) as well as local rearrangements to form longitudinal contacts.[32,33] Tight longitudinal contacts maintain head-to-tail interactions with two other actin monomers in F-actin, while lateral contacts are limited (Figure 2c). F-actin stabilizers such as jasplakinolide and phalloidin increase these lateral contacts by binding within an internal pocket[37−39] (Figure 2c). Each filament subunit is rotated by 166° in unstrained filaments, which therefore have the appearance of a double-stranded right-handed helix (Figure 2d). The N-terminal region is acidic and intrinsically disordered. The main points of structural flexibility within F-actin are in the longitudinal contacts between the D-loop and the C-terminal tail (Figure 2c). Twisting of the filament (Figure 2d) can occur upon binding of protein partners (such as cofilin[40−43]), exploiting internal flexibility. Cooperativity and long-range communication within the filament are promoted by such types of actin binding

DOI: 10.1021/acs.chemrev.9b00264
Chem. Rev. XXXX, XXX, XXX−XXX

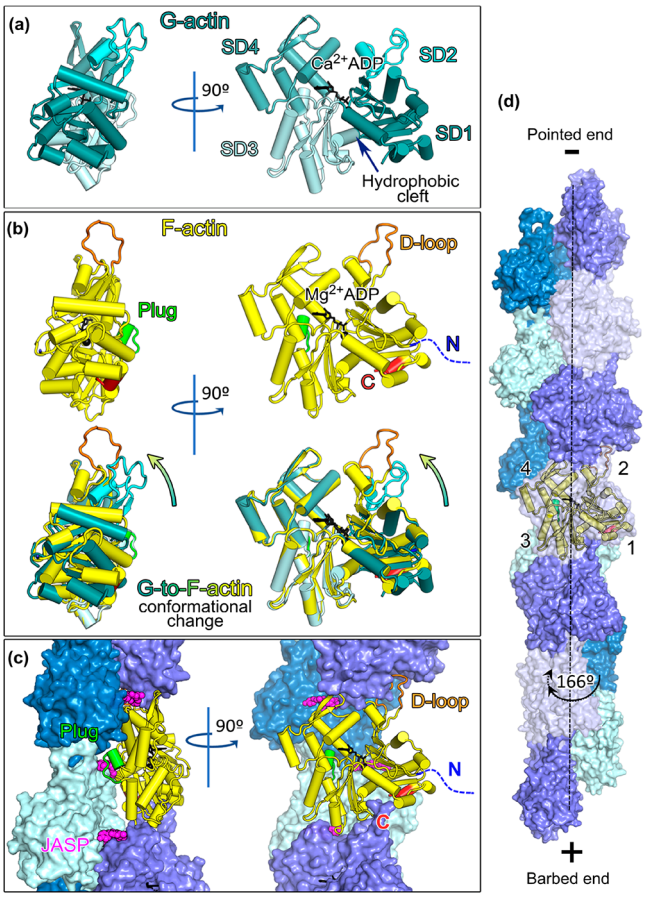

Figure 2. Actin structure. (a) Crystal structure of G-actin (PDB ID 1J6Z[34]) in two orientations. The G-actin molecule is composed of four subdomains (SD1−SD4). A cleft between SD2 and SD4 forms the nucleotide binding pocket. The hydrophobic cleft between SD1 and SD3 is shown with an arrow. (b) Upper part, Structure of a single actin molecule within the actin filament. Lower part, Superimposition of G-actin and F-actin (PDB ID 5ONV[33]). The structures are superimposed on SD3 and SD4. SD1 and SD2 change their orientations (shown with the arrow) upon actin incorporation into the filament. (c) The filamentous actin (F-actin) structure is stabilized by interactions between actin subunits (protomers) in a head-to-tail manner. Each actin subunit forms longitudinal contacts with two neighboring protomers. The plug is a loop connecting actin SD3 and SD4.[35,36] This structural element creates important interstrand lateral contacts with the SD1 and SD2 domains of the neighboring actin molecules within F-actin. Jasplakinolide (JASP) binds and stabilizes the lateral contacts. (d) Actin forms a double-stranded filament with 166° helical twist (arrow). Binding of partners or strain applied on the filament can modify this twist (dotted line). F-actin pointed (−) and barbed (+) ends are labeled.

proteins,[44] as well as multisubunit binding proteins, such as tropomyosin.[45] Actin filaments have a polarity, and their ends (called the plus and minus ends) are distinct from one another. This polarity of actin filaments is important both for their assembly and in establishing a unique direction of myosin movement relative to actin.

1.2.2. Myosins: A Conserved Motor Domain Superfamily with a Variable F-Actin Binding Surface. The design of the motor portion of myosin that generates force and interacts with F-actin is conserved in all classes of myosin that have been studied. It contains **three coupled sites**: the **ATP hydrolysis site** and the **actin binding surface** which are both allosterically connected to the **lever arm**. This lever arm corresponds to the C-terminal sequence of the head (Figure 1a) that is designed to amplify motor domain rearrangements. Several classes of myosins have an extension prior to the motor domain (N-terminal extension), which can participate in the control of the lever arm position.[39,46] The first part of the **lever arm**, at the C-terminus of the motor domain, is known as the **Converter** subdomain and is extended by a variable number of calmodulin (CaM)/light chain[47] binding sites, depending on the myosin class. The Converter is the most mobile of the four motor subdomains, and its swing drives force generation during the motor cycle.

Further extensions of the lever arm can be found in some classes of myosin, including single stable alpha helices (SAHs) in class VII and X myosins.[48,49] Following the lever arm, dimeric myosins, such as class II and V, have coiled coils, which are absent in monomeric myosins, such as class I and class III. The C-terminal portions of all myosin classes contain targeting regions that allow interaction with other proteins in the cell or with lipids from biological membranes.[50−52]

Historically, the motor domain had been described as containing three different segments of heavy chain that had been characterized biochemically due to the proteolysis of two variable loops, called Loop1 and Loop2. The first structure of the motor domain solved by Rayment et al. revealed that the 50 kDa fragment was in fact the major component of two subdomains (Upper and Lower 50 kDa) separated by an inner cleft.[53] Comparison of myosin X-ray structures[53−57] with different ATP analogues bound led to a description of the myosin motor domain[56] in terms of four subdomains [N-terminal (N-term), Upper 50 kDa (U50), Lower 50 kDa (L50), and Converter] and **connectors** between them (Switch-II, Relay, strut, SH1-helix), as illustrated in Figure 3a. The actin binding site contains elements of both the U50 and L50 subdomains, which are separated by a large **internal cleft**, the **50 kDa cleft**, which must close to form a strong actin binding interface.[58,59] While the outer cleft region is part of the surface of the molecule that binds to F-actin, the inner cleft ends with the **Switch-II** connector, near the γP_i of ATP when bound in the active site. Distinct Switch-II conformations occur in myosin depending on interactions at either the nucleotide or actin binding sites that control ATP hydrolysis,[54] P_i release,[60] as well as the movement of the lever arm, known as the **powerstroke**.[58,61,62] They are linked to different extents of cleft closure and therefore to different actin binding surfaces with distinct affinity for the filament.

Rearrangements within the motor domain are transmitted to the Converter by two highly deformable connectors: the **Relay** (an extension of the L50 subdomain) and the nearby **SH1-helix** (at the periphery of the N-term subdomain). The sequence of the connectors is conserved in the superfamily, and the control of their structural changes by the three allosteric sites (nucleotide binding, actin binding, and lever arm) is at the heart of motor function. Another critical element to control rearrangements within the motor is the **Transducer** (the central β sheet and associated loops), which can adopt distinct conformations that directly affect both the active site and the inner cleft of the motor[58] (Figure 3a). Finally, the **Strut** connects the U50 and L50 subdomains and assists in cleft closure during the motor cycle.[36,58] It is currently poorly known how sequence differences in the connectors, the Transducer, or within the motor domain might participate in tuning motor function. A recent study of the divergent

DOI: 10.1021/acs.chemrev.9b00264
Chem. Rev. XXXX, XXX, XXX−XXX

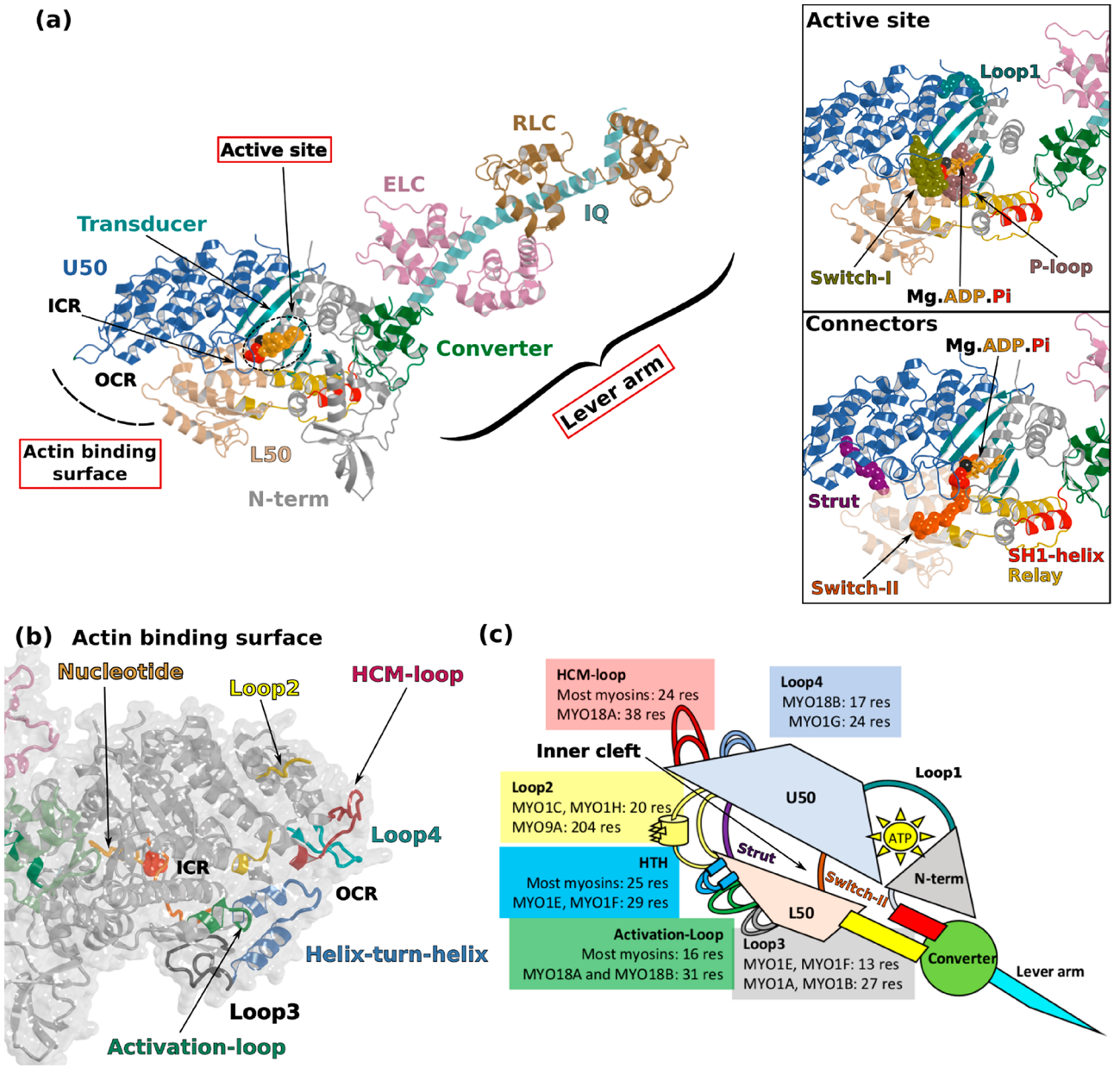

Figure 3. Essential elements of the myosin motor domain. Myosins are allosteric machines containing three major sites: the actin binding surface, the active site that binds and hydrolyzes ATP, and the mechanical element called the lever arm. These sites are illustrated in a cartoon representation of scallop myosin 2 in the Pre-powerstroke state (PPS) (PDB ID 1QVI[63]). (a) Left, the subdomains of the motor domain are colored as follows: N-terminus (N-term), dark gray; upper 50 kDa (U50), blue; lower 50 kDa (L50), amber; Converter, green. The lever arm includes the converter and the IQ helical region (cyan), that protrudes from the converter and binds the essential and the regulatory light chains (ELC and RLC, respectively). Top right, the active site comprises the P-loop and Switch-I that bind the nucleotide. Bottom right, the four connectors between these subdomains are shown. Switch-II (orange) changes conformation depending on the hydrolysis state of the nucleotide. The Strut (purple) links the U50 and L50 subdomains. The SH1-helix (red) and the Relay (yellow) are two structural elements that are cooperatively linked to the converter. (b) The different elements of the actin binding surface are represented: HCM-loop, dark red; Loop4, cyan; Loop2, yellow; helix-turn-helix (HTH), dark blue; Activation-loop, green; Loop3, black. These elements are organized around the internal cleft, which can be subdivided in two regions: the inner cleft region (ICR) near the active site and the outer cleft region (OCR) near the actin binding surface. (c) Schematic diagram of myosin with its different connectors and loops. The length variability of the actin binding loops is indicated among the different human myosin classes.

Plasmodium falciparum MyoA (PfMyoA) myosin has shown how subtle sequence adaptations in the connectors can modify the force generation mechanism.[46]

The **$_{\text{Myosin}}$actin binding surface ($_{\text{M}}$ABS)** is composed of five actin binding loops of variable length and composition as well as a more conserved helix-turn-helix (HTH) structural element of the L50 subdomain (Figure 3b). Thus, while the motor domain design is conserved, the actin binding surface is quite variable among myosins. This raises the possibility that this variability in the interactions with F-actin is critical for tuning the motor properties within this superfamily.

1.3. How Is Force Generated?

1.3.1. General Principles in Force Production by Cytoskeleton Molecular Motors. A linear motor protein

DOI: 10.1021/acs.chemrev.9b00264
Chem. Rev. XXXX, XXX, XXX−XXX

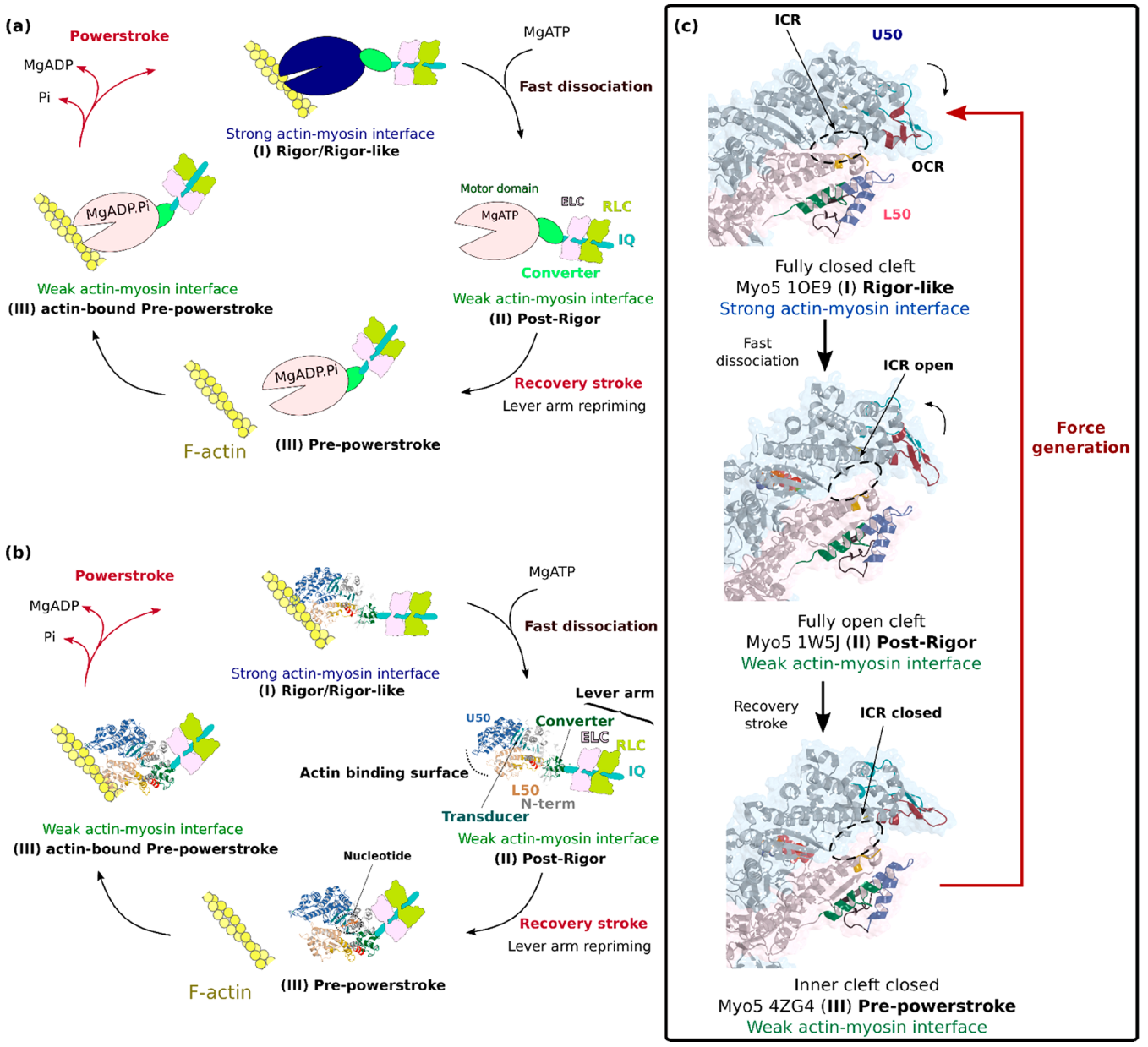

Figure 4. Basic force-generating cycle and myosin crystal structures. (a) The conserved elementary motor cycle (actin-activated ATPase cycle) for the myosin superfamily is comprised of three major states that differ in their nucleotide binding state, their affinity for F-actin, the status of the internal cleft within the motor, and the lever arm orientation. In the Rigor state (I), the myosin is strongly associated with actin with the cleft closed and the active site contains no nucleotide. Binding of ATP triggers cleft opening and dissociation from the actin filament, creating the Post-Rigor (PR) state (II). After an isomerization that allows ATP hydrolysis, the motor is in the Pre-powerstroke (PPS) state (III), with the lever arm up, and has a weak affinity for the filament. The Pre-powerstroke state is the first state that interacts with F-actin to initiate a powerstroke. Association with the filament triggers conformational changes that lead the weakly associated PPS state to reform the strong actin−myosin interface (Rigor) by closing the cleft, during which the hydrolysis products (P_i and MgADP) are released, the lever arm swings (powerstroke), and force production occurs. (b) Known myosin structural states are shown for scallop myosin 2 (ScMyo2) in the force-generating cycle. The myosin subdomains and connectors have been colored as in Figure 3a, and the IQ region with the two light chains (ELC and RLC) bound is shown schematically to better visualize the lever arm reorientation. The PDB IDs of the structures used for the cycle are 2OS8[84] (Rigor-like), 1SR6[85] (Post-Rigor), and 1QVI[63] (Pre-powerstroke). (c) The internal cleft and actin binding surface are depicted for states populated during dissociation and repriming of the motor with the Rigor, Post-Rigor, and Pre-powerstroke states of Myosin V (top to bottom).

can move itself along a track or produce force to deform membranes or contract track networks. The **powerstroke** of these sophisticated ATP-powered machines is a large-amplitude structural reorganization of the motor when bound to the track—that in essence produces mechanical work. The motor must adopt a stable primed (i.e., **Pre-powerstroke**) conformation when unbound to the track. In the case of myosin, F-actin is the track. The powerstroke is triggered and controlled by actin-driven conformational changes that govern transitions to the states that have higher and higher affinity for the track. The last transition of the powerstroke on actin in which MgADP is released is generally, but not universally,[64−66] linked to an increased affinity of myosin for actin. The rate of this transition that controls ADP

DOI: 10.1021/acs.chemrev.9b00264
Chem. Rev. XXXX, XXX, XXX−XXX

release is key to tuning the duty ratio and varies greatly among myosins.[3,13,14] It is a transition that modulates the duty ratio under load and can be tuned to create a myosin that is a more effective anchor on actin than it is a transporter.[67,68] Thus, motor/track interactions are coupled to the directed movement of the force-generating mechanical elements.

The ATPase activity of the unbound motor is intrinsically slow due to slow dissociation of P_i and ADP in myosins. Thus, interactions with F-actin trigger the powerstroke by accelerating these intrinsically slow product release steps, which is coupled to transduction of the chemical energy from the ATP into mechanical work along the track. Along the cycle, ATP binding, ATP hydrolysis, and sequential release of hydrolysis products (P_i and then ADP) are all key transitions in the motor cycle that induce distinct structural states of the motor that have different affinities for the actin track, allowing attachment/detachment of the motor domain. States that are detached from the filament are important as well, since the motor must be reprimed by ATP binding and hydrolysis before force can be produced again.

Early mechanical models of how the actin−myosin interaction might generate force were based on studies of force development by striated muscle but captured many features that we are now trying to understand in light of the current structural and enzymatic data on many myosin classes. In 1957, A. F. Huxley proposed a model that was essentially a Brownian ratchet.[69] It proposed that the polarity of the actin filament generated preferential sites of attachment for myosin and that myosin binding to those sites rectified Brownian motion, thus generating force. While the model was overly simplistic, it made the point that the initial stereospecific binding of myosin to actin is the first component of force generation. Later work from Huxley and Simmons (1971)[70] involving the response of muscle to rapid length changes made it clear that the force generation must take place in multiple transitions, which we now understand to be transitions coupled to swinging of the myosin lever arm (powerstroke) following the initial binding of myosin to actin. However, we have only a few insights into the nature of the actin−myosin interface as it transitions between the force-producing states, or how changes in this interface are coupled to swinging of the lever arm, as will be presented below.

1.3.2. The Motor Cycle of Myosin Motors. Early kinetic studies of the motor/track interactions have defined the Lymn−Taylor basic actin-activated ATPase cycle (or motor cycle) of myosin[71] (Figure 4a). Myosin detaches from the track upon ATP binding and then undergoes a rapid isomerization. ATP hydrolysis (which is reversible in Myo2[72−74]) stabilizes the Pre-powerstroke state, a conformation of the motor that has a weak affinity for F-actin. Reassociation to F-actin triggers the release of P_i followed by ADP, increasing the affinity of the motor for the track, which is highest when no nucleotide is bound (Rigor state) for the vast majority of myosins.

As noted above, early studies revealed that the process of force generation must consist of several components.[70] This led to proposals that some type of reorientation of the myosin motor (or part of the motor) on actin would be the essence of force production.[75,76] This hypothesis was refined and became the **swinging lever arm model**[77] of force production once a high-resolution structure of myosin was available.[53] Evidence for this model was obtained in the mid to late 1990s by multiple experimental approaches,[78−81] when it became clear from structural studies that the probes to follow this rearrangement had to be placed on the lever arm in order to detect significant movements.[53,57,82]

Atomic structures of myosin in the absence of track binding have led to an understanding of what distinguishes weak and strong binding states,[58,83] as well as which conserved structural elements in this allosteric motor play essential roles to trigger the swing of the mechanical element in response to the status of the nucleotide binding site or the actin interface. In Figure 4b, the main structural states are placed within the **Lymn−Taylor cycle**, depicting the required structural changes occurring for each transition.

Starting from the nucleotide-free or **Rigor state**, in which the motor and the track interact strongly, the energy of ATP binding is used to create strain within the transducer region, which is coupled to opening of the internal (50 kDa cleft) cleft and rapid detachment of myosin from F-actin without appreciable mechanical movement of its lever arm. This initial ATP state of the motor is known as the **Post-Rigor state**. Fast dissociation is linked to opening of the large internal cleft in the motor upon ATP binding that separates the two main components of the actin−myosin interface. After detachment, the ATP-bound motor rapidly isomerizes to a state that can hydrolyze ATP and in which the lever arm is primed. This isomerization is called the **Recovery stroke**. All-atom molecular dynamics simulations have recently indicated that lever arm repriming would be mostly driven by thermal fluctuations and eventually stabilized by Switch-II interaction with the nucleotide in a ratchet-like fashion.[86] Several transient states are thus rapidly explored, ultimately allowing the population of a state in which hydrolysis of ATP can occur, the **Pre-powerstroke (PPS) state** (Figure 4b). This PPS state has been trapped in crystals with ADP.P_i analogues.[54,55,57,87] Hydrolysis stabilizes this primed state that has a weak affinity for the actin track. The stability of this PPS state is linked to the trapping of the hydrolysis products: Inorganic phosphate (P_i) and MgADP, which are tightly coordinated until binding to actin initiates force generation. Once myosin does interact with actin, the PPS state can only associate weakly[88,89] until surface loops at the actin interface position the myosin motor to interact stereospecifically with actin (likely via electrostatic steering). These actin interactions induce a conformational change in myosin to bind more strongly to actin, initiating force generation.[60] This first transition allows not only the formation of a stronger actin binding interface and a small change in lever arm swing but, importantly, opens a back door[90] to facilitate the release of P_i from the active site. Further, rapid changes in the actin interface[91,92] are coupled to the major component of the powerstroke (lever arm swing) to generate more force. Thus, strengthening of the interactions with F-actin is allosterically communicated to the nucleotide binding site and the lever arm. This major component of the powerstroke also gates the reaction, since the release of Pi is irreversible under unloaded conditions. This is followed by an additional lever arm swing associated with ADP release,[78,93] which may be driven either by much smaller changes at the actin interface[39,94,95] or simply by the relaxation of the transducer that is coupled to nucleotide release.

Overall, several transitions of the motor are controlled by distinct sets of actin−myosin interactions and their timing is essential to define the force the motor can produce, in particular under load. The interaction with actin is disrupted when ATP binds to the empty active site, causing the myosin

DOI: 10.1021/acs.chemrev.9b00264
Chem. Rev. XXXX, XXX, XXX−XXX

dissociation restarting the cycle. As stated above, the duty ratio characterizes the time the motor stays in the actin-bound force-generating states compared to the whole cycle.[3,13,14] This important parameter for tuning the motor function depends on the kinetics of the transitions into and out of the force-generating states and their load dependence. Low-duty-ratio motors are adapted to high velocity by allowing fast cycling of motors as an assembly. The low duty ratio is achieved by a slow rate of entry into the first force-generating state on actin. Processive and force sensing motors[3,13,14] must have a high duty ratio, which is generally achieved by slowing the rate of ADP release from myosin while bound to actin under a resisting load.

1.3.3. Main Questions Regarding Force Production by the Myosin Motors. The three main components in myosin motors (Figure 1a), the motor itself, its lever arm but also the tail which plays a critical role in defining how motors are assembled, are all critical to define the cellular functions a motor is best designed to accomplish. All three parts of the motor are critical to stabilize the inactive state of the motor, since they are then involved in internal autoinhibitory interactions.[6,10−12] These regions also play major roles in coordinating the spatial and temporal recruitment of motors and their assembly.[6] In cells, motor activation must indeed be spatially and temporally controlled. Cargo/partner binding via the tail or N-terminal extensions of myosin motors define their specific cellular recruitment, but whether signaling is required to destabilize the inactive state prior to recruitment is currently unknown. The role of the lever arm is to define the step size and orientation of the force produced.[96−98] In Myosin X, the lever arm and its dimerization region favor stepping on parallel actin filaments, which is adapted for its function in filopodia,[99−102] rich in such actin bundles.

Brownian motion and electrostatic steering are key in directing the initial weak interactions of the motor with actin. Strain exerted on the landing head favoring or disfavoring the first transition allowing the engagement of the head in the powerstroke is critical to promote either force generation or detachment of the head.[103,104] Thus, myosin motors use both rectification of Brownian motion[105] and directed movement via lever arm swing to produce force. The docking site on actin of a lead head of a two-headed, processive motor is dependent on the actin binding sites best positioned for productive binding that allow the motor to engage in strong interactions, and is further constrained by the design of the myosin lever arm.[96−99]

The motor characteristics defining the force produced and its sensitivity to load are intrinsically linked to the timing of the transitions the motor domain undergoes when bound to F-actin and the extent of lever arm movement associated with each transition. Little is known at present about how F-actin controls these conformational changes. It is critical to understand how interaction of weaker structural states can drive motor rearrangements and lead to stronger binding interfaces. The role of the track is highlighted by the fine-tuning that actin isoforms can play in some myosin kinetics.[106] In cells, F-actin filaments can be bound to diverse tropomyosin isoforms that are also important modulators of myosin functions.[107−109] Tuning the kinetics of the transitions and the energy barrier for their reversibility under load is at the essence of the properties these motors can provide within a cell. Since the track is conserved, how much of motor adaptation comes from internal allosteric tuning versus variations in the actin−myosin interactions is currently unknown.

1.4. Structural Studies Provide Precise Mechanistic Insights on How Force Is Generated

Multidisciplinary research is essential for gaining insights into chemo-mechanical transduction and to define the properties that distinguish members of the myosin superfamily. Structural data is particularly insightful, as they provide atomic details about the motor rearrangements. Previous studies on the unique motor that goes in the reverse direction—Myosin VI—clearly illustrate how structures can shed light on motor mechanisms and adaptations that allow new functions.[7] The reverse directionality in this motor mainly comes from the redesign of its Converter with the adjacent 40-residue long insert, which repositions the lever arm in the opposite direction.[7,110] The measured size of the Myo6 powerstroke appeared to be too large to be compatible with a lever arm swing. High-resolution structures obtained by X-ray crystallography revealed that the structural elements within the Myo6 Converter undergo conformational changes between the pre- and poststroke states, a rearrangement that leads to the unexpectedly large lever arm swing.[7,111]

Furthermore, it was a new structural state of Myo6 that provided the first structural insights into the rearrangements the motor undergoes to initiate force production and to release P_i from the active site.[60] Functional studies based on these insights confirmed that P_i release occurs from a structural state in which cleft closure has not yet occurred. This study represents a major milestone in deciphering how the powerstroke is directed by actin binding. Cryo-electron microscopy (Cryo-EM) structures of a number of myosin classes are also milestones in this understanding, as the resolution achieved provided details for the contacts that occur in strong binding states of the motor.[36,39,95]

Further structural studies are essential to gain an understanding on how the motor produces its mechanical work and how mutations may enhance/decrease the intrinsic force produced and cause human diseases, such as in hypertrophic or dilated cardiomyopathies.[112] The limitations of current models stem from our profound lack of understanding of the actin−myosin contacts in weak and strong actin-bound states that drive force generation. We will examine the conundrum of where in the motor domain are the main sequence differences that are critical for kinetically tuning the transitions of the powerstroke to achieve different motor properties. The variability in the actin binding surface ($_M$ABS) among myosin family members is likely part of the answer due to its role in altering the kinetics of the actin-driven transitions. However, lack of sequence conservation could also reflect a lack of functional significance of these variable regions. For an allosteric enzyme, such as myosin, it is thus not trivial to decipher how sequence differences within the motor domain have an impact in modulating myosin activity.[66,113] Studies on alternative exons in *Drosophila* muscle myosin 2 have begun to provide insights in this regard.[114−116] Sequence differences responsible for tuning the motor may also reside in locations in the motor that have yet to be identified, or in variable sequence extensions of the motor that influence the swing of the lever arm.[39,46] Thus, a full understanding of the evolutionary tuning of myosin motors as well as the impact of many human-disease-causing mutations awaits a more detailed understanding of how actin and myosin interact throughout the

DOI: 10.1021/acs.chemrev.9b00264
Chem. Rev. XXXX, XXX, XXX−XXX

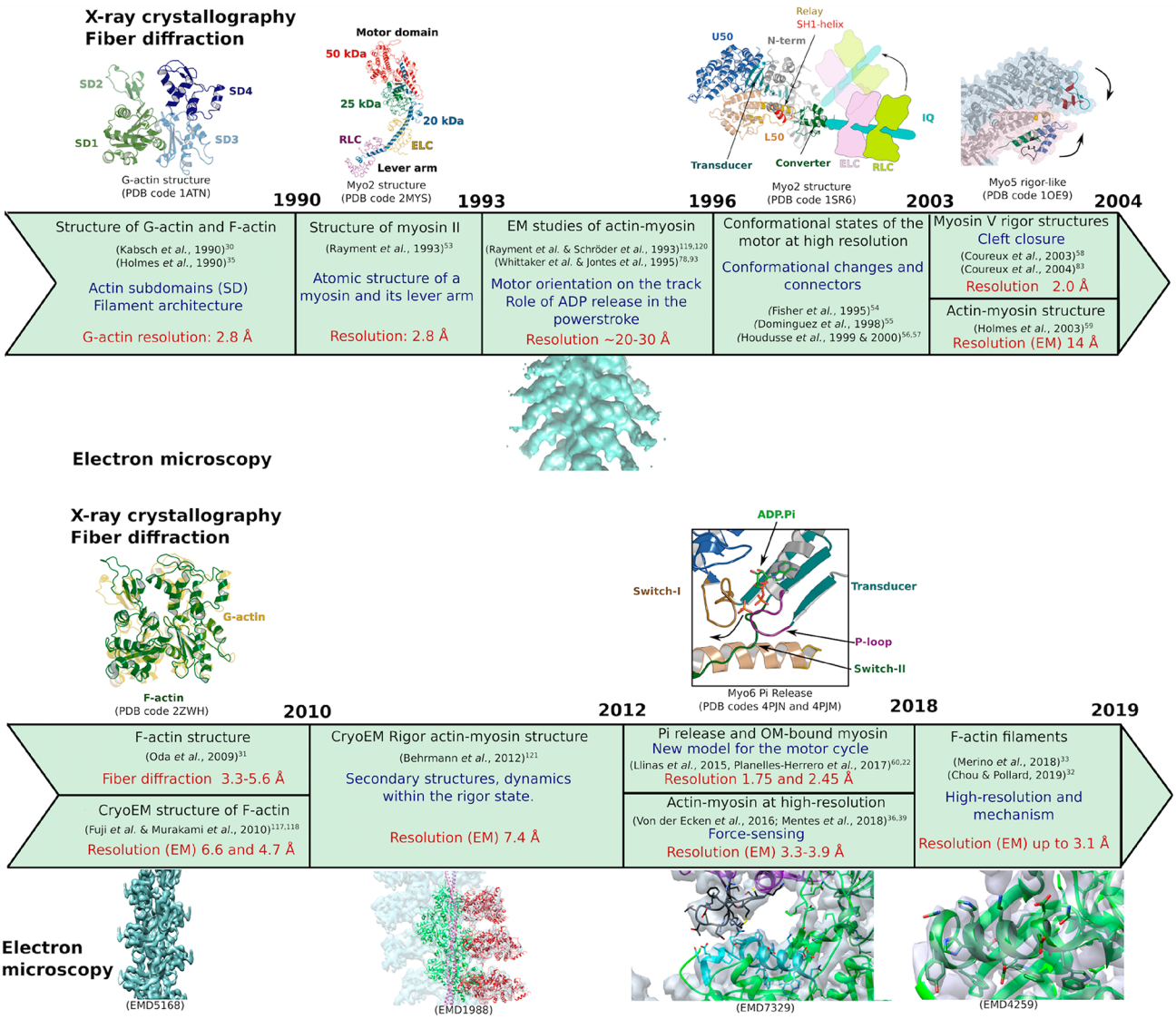

Figure 5. Illustrated time line of the structural biology contributions that lead to current understanding of the actin−myosin motor mechanism. Contributions obtained by X-ray crystallography and fiber diffraction are illustrated on the top, while contributions from electron microscopy are illustrated on the bottom.

force-generating cycle. This review will outline the current knowledge and gaps in knowledge in achieving this understanding.

2. EARLY STUDIES ON HOW MYOSIN INTERACTS WITH F-ACTIN

2.1. From X-ray Studies to the Cryo-EM Revolution: Milestones in Understanding the Actin−Myosin Interactions

Achievements in understanding how myosin produces force on F-actin has been a long-standing endeavor, always searching for higher resolution in depicting their structural states. While the structure of F-actin had been described at 8.4 Å resolution by the use of X-ray fiber diffraction of oriented F-actin gels[35] in 1990, flattening of the monomer upon its incorporation into the filament was described in 2009 with studies at 3.3 × 5.6 Å resolution.[31] In 2010, the resolution of Cryo-EM studies for F-actin filaments was sufficient to describe the secondary structure, but this was still limited to 4.7 Å resolution in the best resolved regions.[117,118]

In 1993, EM studies of the actin−myosin rigor complex at 30−20 Å resolution[119,120] described the rough orientation of the motor when bound to F-actin as well as the downward position of the lever arm (Figure 5).[119,120] They also recognized that myosin binds at the junction between two adjacent actin monomers in the long pitch helix. When interpreted with the myosin crystal structures available at the time (Post-Rigor)—a state of low affinity for F-actin—they described the myosin structural elements predicted to interact with F-actin but the interface could not be properly described. Indeed, it was not possible to guess the structural changes in the motor or in the track needed to create a proper interface without steric clashes. In 2003, using zero-loss energy-filtered imaging, a Cryo-EM map up to ~10 Å resolution was published for the Rigor state[59] back to back with the structure of Myosin V in a previously unseen **Rigor-like state** (crystallized without actin and no nucleotide bound).[58] This data convincingly described that the conformation of myosin

DOI: 10.1021/acs.chemrev.9b00264
Chem. Rev. XXXX, XXX, XXX−XXX

of highest affinity required a full closure of the **internal cleft** between the L50 and U50 subdomains (50 kDa cleft). Nine years later, the first sub-nanometer resolution structure of the rigor complex of an actin−tropomyosin−myosin complex containing *Dictyostelium discoideum* myosin-1E (DdMyo1E)[121] was reported. This structure, solved at 7.4 Å best resolution, provided the first visualization of the secondary structural elements in a Rigor state and the conformation of most loops involved in actin binding.[121] However, the resolution was still insufficient to describe the contacts at the interface and be sure that all actin binding elements (in particular Loop2) were indeed involved in the rigor interface.

The last step of the powerstroke, ADP release, was also studied by Cryo-EM by comparing decorations of actin−myosin in Rigor and saturated with MgADP. These structures revealed that an ∼30−35° swing of the lever arm occurs for smooth muscle myosin II[78] and myosin I.[93] The resolution in these studies (30−20 Å) was not sufficient to observe the main differences in the motor domain, although computer-assisted docking and difference maps were used to suggest that an overall reorientation of the motor would occur as well as rearrangements in specific sites of the motor domain.[122] Higher-resolution Cryo-EM studies of Myo5 (∼7.6 Å),[94] Myo1b (3.2, 3.8, and 3.9 Å),[39] and Myo6 (4.6 and 5.5 Å)[95] bound to F-actin have shown that the actin binding interface does not change much, if at all, upon ADP release and that there is no reorientation of the motor on the track during this transition.

Diffusion limited binding of nucleotide-free Myosin V provides evidence that this myosin does not require major conformational changes to associate with F-actin.[58,123] This is not true for *Dictyostelium* Myosin II or Myosin VI, and in fact, the Rigor-like states crystallized for these myosins do not have a fully closed cleft.[110,124] Cryo-EM data at 3.9 Å resolution for the human cytoplasmic non-muscle myosin 2c (NM2c) actin−myosin rigor complex[36] showed later that the cleft is fully closed in Rigor and that the Rigor-like structure of Myosin V in the absence of F-actin truly corresponds to the Rigor (myosin-bound) state.[58]

Atomic coordinates at 2 Å resolution of Rigor-like and ATP-bound states of Myosin V revealed in detail the major changes occurring in Myosin V upon ATP binding.[58,83] Nucleotide binding stabilizes the twisted conformation of the **Transducer** (central β sheet and associated loops, Figure 3a), allowing Mg^{2+}ATP coordination via two elements of the nucleotide binding site, namely, the **P-loop and Switch-I** (Figure 3a), that cannot occur in the Rigor structure in which the open active site can only bind nucleotide weakly. While the cleft between the U50 and L50 subdomains is closed in Rigor, it is fully open in the Post-Rigor state (Figure 4c), that promotes dissociation of the motor from F-actin. Large separation between two major sites of the actin interface describe how myosin can adopt a weak (μM) and strong (nM) actin binding interface. The mechanism of quick dissociation of the motor without any lever arm movement was thus revealed at 2 Å resolution by direct comparison of the Rigor-like and Post-Rigor structures of Myosin V (reviewed in refs 62 and 125). The Transducer also plays a critical role in closing the internal cleft during the powerstroke on F-actin in coordination with events in the active site.[58,62,94] Different twists of the Transducer beta-sheet can affect the relative position of the P-loop (which is part of the N-term subdomain) and Switch-I (which is part of the U50 subdomain), and thus may control the release of MgADP from the active site. While the ADP is held in the P-loop, Mg^{2+} and ADP must indeed interact with Switch-I for strong binding.[62,83,94,126,127]

The field has greatly benefitted from the recent Cryo-EM revolution operated in recent years, and the actin−myosin structure in Rigor has been solved at near-atomic resolution (3.9 Å) with the non-muscular myosin 2c (NM2c) by Stefan Raunser and colleagues.[36] This structure was the first to allow building of the side chains in the electron density map and to describe precisely the contacts between myosin and the actin filament. The near-atomic structure of the Myo1b actin−myosin complex in Rigor (3.9 Å resolution) and in the Strong-ADP state (3.3 Å resolution) provided the direct comparison of the interface for different states of this motor upon ADP release.[39] These studies are the most accurate to date for discussing the conservation of the actin−myosin interface among myosin family members.

2.2. Why Is Actin−Myosin a Challenge for Structural Biologists?

The main difficulty in describing how myosin interacts with F-actin is the fibrous nature of the actin filaments that makes it recalcitrant to crystallization. Despite several creative strategies since the early 1990s,[128−130] it has not been possible to produce an actin oligomer of defined size for crystallization with myosin bound. Cryo-EM is thus the only method available at present to study the structure of this complex, and the resolution of the electron density map has been improving greatly by recent advances in detector hardware and image-processing software. However, the dynamic nature of the complex probably limits the current achievable resolution, since the motor and the F-actin track may explore several states in a particular decoration. The flexible nature of the filament and the need of full homogeneous decoration requires persistent trial and error assays to obtain an actin−myosin complex suitable for high-resolution structures. Development of new specific methodologies for structure determination[131] will likely overcome the specific challenges of this system and lead to the best resolution achievable.

The average resolution cited previously for Cryo-EM structures[36,39,95] is in fact best for the F-actin filament and decreases for regions of myosin further away from the interface. Lower average resolution maps (5−6 Å) are not always sufficient to identify the position of Cα and thus the precise conformation of the motor connectors. The modeling of several elements of the interface cannot be described accurately from the electron density map in these studies; these limitations are not always reflected in the coordinates of these structures, which are often completed by model building despite lack of density. Higher resolution (better than 4.0 Å) is essential to define most of the side chains responsible for the contacts at the interface. While the knowledge acquired from X-ray structures of each protein, including actin binding loops, helps in interpreting these electron density maps, direct study of the maps, rather than the model built from the map, is critical to describe the validated structural information.[132,133] The challenge is to obtain high-resolution structural states for each of the subclasses explored by the system due to its dynamic nature. This is likely the limiting factor in resolution when the structural changes are particularly small in amplitude or highly dynamic. Note that other cytoskeleton motors are even more difficult to study. For dyneins, the track binding region and the motor domain are linked by elongated and

DOI: 10.1021/acs.chemrev.9b00264
Chem. Rev. XXXX, XXX, XXX−XXX

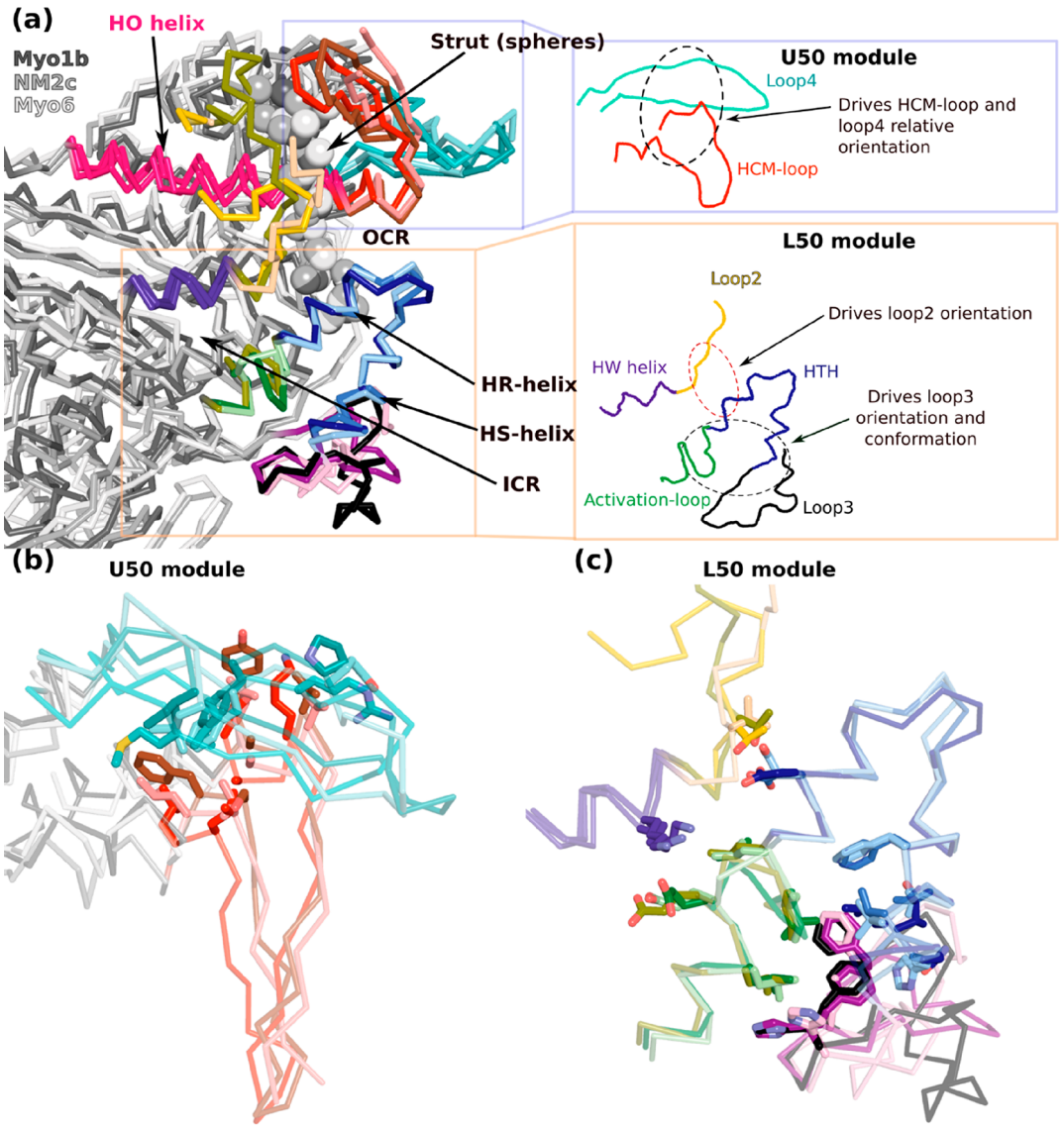

Figure 6. Myosin elements involved in actin binding. (a) Left, comparison of the actin binding surface ($_M$ABS) of non-muscle Myosin 2c (NM2c, EMD8165[36]), Myosin 1b (Myo1b, EMD7331[39]), and Myosin 6 (Myo6, EMD7116[95]) from actin−myosin Rigor EM structures. The actin binding elements of the motor domain (gray) are colored as follows: HCM-loop, red; Loop4, cyan; Loop2, yellow; HO-helix, violet; helix-turn-helix (HTH), dark blue; Activation-loop, green; Loop3, pink/purple/black. The Myo6, Myo2, and Myo1 structural elements are distinguished by a color gradient (from a lighter to a darker color, respectively). Residues that belong to the strut are indicated as balls. Right, schematic representation of these actin binding elements organized in two modules, the U50 and L50 modules, as well as the interactions existing within them. The dashed lines correspond to contacts between the actin binding elements (shown in detail in parts b and c). (b and c) Shown are the side chains of residues involved in the interactions between the actin binding elements within the U50 and L50 modules, respectively.

flexible structural elements. Myosin has large subdomains and explores conformational changes of large amplitude within its motor cycle, making it relatively easy to distinguish different states of the motor.

3. THE STRONGLY BOUND ACTIN−MYOSIN INTERFACE

Structural regions of F-actin and myosin that define the rigor interface have been approximately described since 1993, when the first myosin X-ray structure[53] became available. A rough description of the rigor interface (reviewed in Milligan 1996),[134] namely, the regions that likely are in contact on either side of the interface, emerged from early EM studies[119,120] that were interpreted using X-ray structure coordinates.[53] However, no details of the actin−myosin contacts formed were possible (see part II of this review). Other actin−myosin structures solved recently describe the overall features of the Rigor state of smooth muscle myosin-II (at 6.0 Å average resolution)[135] and fast skeletal muscle myosin-II (5.2 Å best resolution).[136] The description of the interface we are providing in this review is based on the highest-resolution maps that have since become available.[36,39,95]

The highest-resolution structures of NM2c and Myo1b[36,39] bound to F-actin are indeed key achievements for the field, which allow us to assess for the first time how conserved the strong actin−myosin interface is among family members. Another actin−myosin study has been performed at lower resolution, providing the Rigor and Strong-ADP states of Myo6 (at 4.6 and 5.5 Å best resolution, respectively).[95] To

DOI: 10.1021/acs.chemrev.9b00264
Chem. Rev. XXXX, XXX, XXX−XXX

compare these structures, the electron density maps, rather than the model coordinates that interpret them, were studied here to avoid overinterpretation. These results allow a broad discussion on the conformational structural adjustments required to form the rigor interface and the conservation of contacts with F-actin among different myosins. Interestingly, these three myosins are representative of functionally distinct classes of motors, since they are adapted for force sensing (Myo1), low duty ratio/contractile (NM2c), and reverse direction processive movement (Myo6).

3.1. The Myosin Side of the Interface—General Characteristics of the Actin Binding Surface ($_M$ABS)

On the myosin side, the **$_{Myosin}$actin binding surface ($_M$ABS)** consists of two main sites found on the L50 and U50 subdomains (Figure 6a), which can drastically change in orientation depending on the closure of the internal cleft that separates these subdomains (Figure 4c). This cleft closure mechanism induced by actin binding is the major element that distinguishes weak and strong binding states. The crystal structures of myosin unbound to actin provide high-resolution information on the $_M$ABS in different states of the motor cycle as well as the structural flexibility of its elements. The variability found for this interface in three Cryo-EM Rigor actin−myosin structures is presented in Figure 6. The most conserved region of the $_M$ABS is the **helix-turn-helix (HTH)** surface whose conformation is highly constrained, as it corresponds to the large surface of the L50 subdomain made of the ^{L50}HR and ^{L50}HS helices.[137] Here, structural variability is only present at the tip, in the short hydrophobic turn between the helices (Figure 6a). The rest of the interface is made of five loops that vary in length and composition (Figure 3c, Figure 6a). **Loop2** is intrinsically disordered and is the most variable. In the majority of the myosin structures solved to date, only the anchorage points are defined in the electron density. Loop2 links the U50 to the L50 subdomains near the strut, a short structural element of defined length, important for closure of the inner cleft near the actin interface. The Loop2 C-terminal end, which is rich in positively charged residues, is anchored to the L50 subdomain, as it ends in the ^{L50}HW helix[137] that spans one side of the internal cleft. On the opposite side of the cleft, the long ^{U50}HO helix[137] follows the C-terminal region of the HCM-loop, also named the TEDS loop after a consensus motif of phosphorylation[138] (Figure 6a). We use the more common nomenclature, "HCM-loop", in this review.

On the U50 subdomain, two variable loops are oriented toward F-actin, the **HCM-loop** and **Loop4** (Figure 6a,b). These loops fold as antiparallel beta-hairpins at their base, with a more flexible loop region of variable length at their tip. Both of them are anchored within the U50 with restricted flexibility at the anchorage points. Communication between these loops also occurs, since they directly interact at their base (Figure 6b).

On the L50 subdomain, three structural elements bind actin: the helix-turn-helix (HTH), **Loop3**, and the **Activation-loop**. The Activation-loop directly precedes the HTH, while Loop3 follows it. The N-terminal sequence of Loop3 serves to anchor it rigidly to the L50 subdomain via beta-sheet-type interactions, and it also makes close contacts with the Activation-loop (Figure 6c). The rest of Loop3, which is where contacts with F-actin can occur, is highly flexible and variable in length and composition (Figure 3c). The Activation-loop is much shorter, but it is also of variable length and composition (Figures 3c and 6c).

In conclusion, the variability in sequence and structure is quite pronounced except for the ^{L50}HTH surface, which raises the question of whether the interactions with the F-actin track that drive the powerstroke are conserved among myosins. This variability in the loop sequences could however correspond to unrestricted parts of these structural elements if most of their sequences do not participate in actin binding. Interestingly, the anchoring points of these loops allow restricted flexibility but also communication between them (Figure 6b,c). With possible variability in the exact way the cleft can close and orient the two main sites of the actin binding surface, the actin surface explored by myosin is large, since the myosin side of the interface is structurally plastic and dynamic. However, the actin binding elements are not independent of each other, which is essential to transmit conformational changes to the rest of the motor. However, predicting of how the actin binding interface might be modified during progression through the powerstroke is currently impossible. It is thus critical to gain insights from high-resolution structures to address these questions.

3.2. Overview of the Actin−Myosin Rigor Interface

In the high-affinity rigor complex, myosin binds an extensive surface of the F-actin filament (Figure 7a) (~1630 Å^2 for Myo1b, ~1740 Å^2 for NM2c), which is consistent with the nM affinity of the complex ($\leq 10^{-8}$ M).[66,139−141] Complementarity in overall shape, interacting hydrophobic surface residues, as well as complementary charged residues all contribute to the formation of this high-affinity interface (Figure 7b). Two adjacent actin subunits of the filament are involved in myosin binding. Thus, the higher affinity of myosin for F-actin compared to G-actin[142] is not only due to the structural changes that distinguish these two actin forms[31] but mainly from the fact that a larger surface can contribute in the polymerized form of actin. Most of the interactions are centered on the subdomain-1/subdomain-3 surface of Actin-1 and extended on the subdomain-2 surface of Actin-2 (Figure 7c).

The contacts between F-actin and myosin can be described as occurring on six adjacent sites that define the footprint myosin occupies on the F-actin surface (Figure 7c). The large primary binding site on F-actin is recognized by the ^{L50}HTH and spans the junction between two adjacent actin monomers in the long pitch F-actin helix (Figure 7c, blue balls). This ^{L50}HTH site is formed by a hydrophobic groove deprived of negative charges (Figure 7b) between the ^{Actin2}D-loop (subdomain-2) and ^{Actin1}subdomains 1 and 3. The adjacent most conserved site extends on ^{Actin1}subdomains 1 and 3 and interacts with the ^{U50}HCM-loop (Figure 7c, red balls). It mainly comprises hydrophobic and a few negatively charged residues on F-actin, complementary to the mainly hydrophobic residues of the ^{U50}HCM-loop (Figure 7b). On the periphery of this central interaction zone (Figure 7c, blue and red balls), three peripheral sites correspond to the interactions that ^{L50}Loop3, the ^{L50}Activation-loop, and ^{U50}Loop4 can make, respectively, with ^{Actin2}Subdomain-1 (Figure 7c, gray balls), ^{Actin1}Subdomain-1 (Figure 7c, green balls), and ^{Actin1}Subdomain-3 (Figure 7c, cyan balls). Finally, additional interactions of ^{Actin1}Subdomain-1 can occur in some rigor actin−myosin complexes with Loop2 and the ^{L50}HW helix next to the central primary region (made of the ^{L50}HTH and ^{U50}HCM-loop).

DOI: 10.1021/acs.chemrev.9b00264
Chem. Rev. XXXX, XXX, XXX−XXX

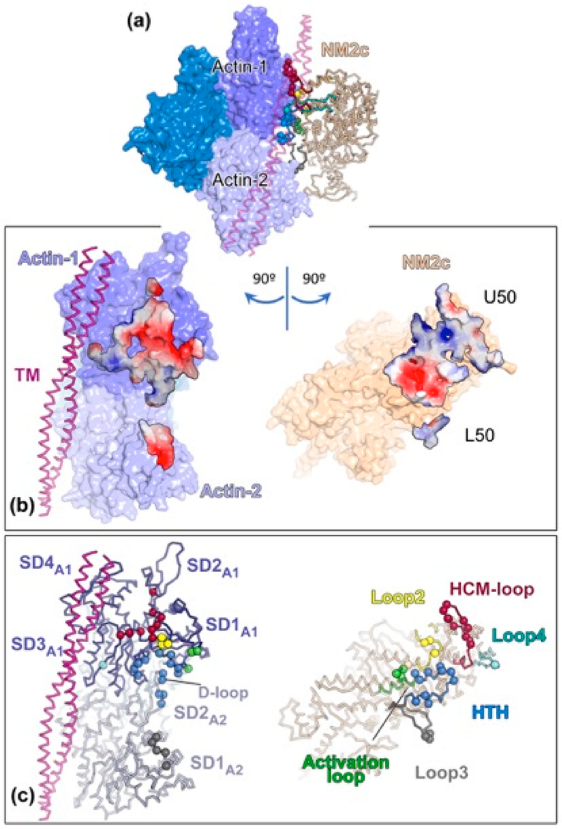

Figure 7. The actin−myosin interface. (a) The non-muscle Myo2c motor domain (NM2c) bound to F-actin (PDB ID 5JLH[36]) (with only three actin subunits) as well as tropomyosin are shown. (b) Actin (left) and myosin (right) surfaces (within a 5 Å distance of each other) are colored according to the surface electrostatic potential distribution (red −5; blue 5 K_bT/e_c). (c) Residues making interprotein contacts (within 4 Å distance) are shown as balls. Right, the myosin actin binding structural elements are shown in different colors. Left, actin residues are colored depending on the myosin structural elements that contact them.

Interestingly, the major binding sites (^{L50}HTH and ^{U50}HCM-loop) at the core of the interface are formed by the surface of F-actin near the intrastrand interactions defined by the D-loop/C-ter interactions, which are the most variable among F-actin structures, as we will describe. This will set the stage to discuss whether binding of the motor during the powerstroke could influence the structure of the filament *per se* and how much dynamics in the filament itself is required for force production.

3.3. The Actin Side of the Interface

Whether or not actin conformational changes occur upon myosin binding has not been easy to assess. Such changes have been suggested, based on early observations that decoration of actin filaments by myosin heads leads to fully decorated as well as completely naked filaments on the same negative stain EM grid,[143] an observation attributed to a cooperative effect.[144] Several lines of experimental evidence indirectly suggest that actin changes conformation and that its dynamics may be an important factor for force generation, as reviewed by Thomas et al.[145] and Galkin et al.[146] Baker and Voth[147] used all-atom molecular dynamics and coarse-grained simulations to probe possible actin conformations. More recently, it has been reported that decoration with Myo5 in the Strong ADP state changes the helical twist of the filament,[94] but this is not the case for Myo1b.[39] The current resolution of Cryo-EM electron density maps needs to be improved to confirm whether changes in the actin conformation could contribute to stabilize different states of the powerstroke.[95] Only minor changes in F-actin are indicated in higher-resolution maps obtained for NM2c and Myo1b,[36,39] and it is possible that the motor in fact selects conformations that F-actin naturally explores. Only indirect observations are currently available to assess whether this flexibility is required for full force generation,[146] and it is not clear when during the powerstroke a change in the F-actin structure occurs. In fact, some of the evidence for a required actin structural change comes from experiments using cross-linking or probes that can themselves introduce bias and perturb the actin structure.[148,149] The highest-resolution structures of F-actin in different nucleotide-bound states[32,33] are the first to provide direct visualization for structural conformational variability within the filament and where changes may occur upon binding of myosin, as summarized below.

3.3.1. F-Actin High-Resolution Structures and Filament Dynamics. The seminal ADP-bound F-actin structure was solved by fiber diffraction reaching 3.3 Å resolution in the radial direction.[31] Two Cryo-EM studies provide details of the interface between subunits and the nature of the interactions that build the filament[32,33] (Figure 8a). Several F-actin structures were solved under different nucleotide conditions[32,33] that depict the structural differences between a young (ATP- or ADP.Pi-bound) and an old (ADP-bound) F-actin structure. Interestingly, the landing rate and run length of Myosin V are higher on young, ADP.P_i filaments, while they are longer for Myosin VI on old, ADP-bound filaments.[150] The ADP.P_i filaments are more rigid than ADP filaments according to their persistence lengths of 13.5 and 9 μm.[151]

Using different γP_i analogues to visualize ATP or ADP.P_i states of the filament, two Cryo-EM studies[32,33] describe how formation of the filament leads to fast ATP hydrolysis in the added subunit.[152] However, the two studies derived different models of the young (ATP- or ADP.P_i-bound) F-actin state. The major changes in these structures occur at the D-loop/C-terminal longitudinal (intrastrand) contacts, which involve the most dynamic regions of the filaments (Figure 8b). In ADP-bound filaments, a variable closed conformation of the D-loop does not interact strongly with the C-terminal peptide of the adjacent actin subunit in both studies.[32,33] An open conformation of the D-loop was reported to be predominantly explored in filaments stabilized by either ADP.BeFx or jasplakinolide with either ADP or ADP.P_i by Raunser et al.[33] This open D-loop configuration makes strong intrastrand interactions with the unwound C-terminal peptide. Raunser et al. suggest that the open D-loop configuration at this interface is only explored in young (more rigid) filaments and would account for the selective recognition of ATP- versus ADP-bound filaments by proteins such as coronin-1.[33] While a high-resolution structure of the F-actin/coronin-1 complex is required to confirm this, the structural-based selectivity cannot be the full story, since several states can be explored for a particular nucleotide, and differences in the dynamics of F-actin are highly dependent on the nucleotide bound. The open D-loop configuration was not observed[32] or was not predominant[33] when ADP.P_i or AMPPNP were bound. Lack of evidence for the open D-loop configuration in AMPPNP and ADP.P_i F-actin filaments led Chou and Pollard[32] to

DOI: 10.1021/acs.chemrev.9b00264
Chem. Rev. XXXX, XXX, XXX−XXX

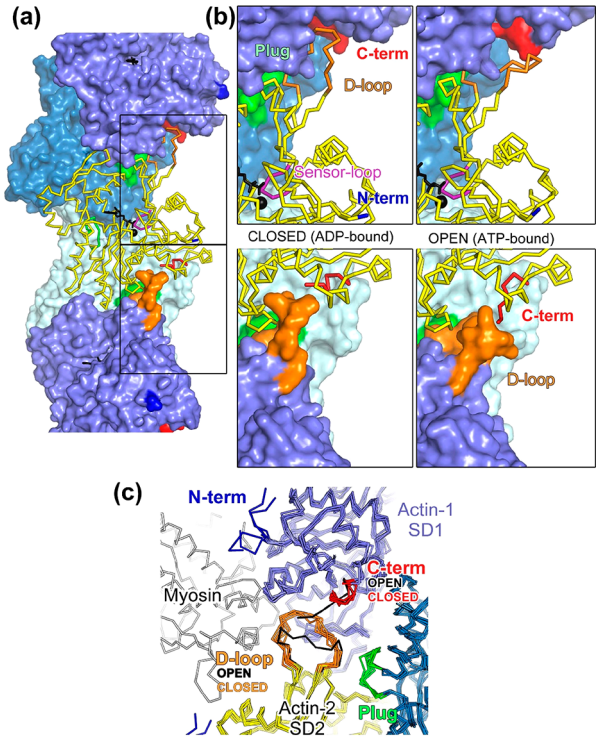

Figure 8. F-actin conformational flexibility. (a) Depicted is an actin subunit (represented in yellow ribbon) surrounded by four other subunits (surfaces) within the actin filament. (b) Close-up view of the interacting regions boxed in panel a. Left, closed conformation of the actin D-loop and C-terminal tail typical for ADP-bound F-actin (PDB ID 5ONV[33]). Right, open conformation of the actin D-loop and C-terminal tail that can be observed in ADP.BeFx-bound F-actin (PDB ID 5OOF[33]) or in ADP, JASP-bound F-actin (PDB ID 5OOC[33]). (c) Conformational differences between F-actin containing structures for the N-terminal and C-terminal regions as well as the D-loop (PDB IDs: 5ONV[33] (ADP-bound F-actin); 5OOC[33] (ADP, JASP-bound F-actin, representing the open ATP-bound conformation of F-actin); 6C1H[39] (Myo1b-bound F-actin); 5JLH[36] (NM2c-bound F-actin); 31288[94] (Myo5-bound F-actin); 6BNP[95] (Myo6-bound F-actin)).

propose that subtler changes distinguish ATP- versus ADP-bound F-actin states, which would differ mainly in the closed D-loop flexibility, and not on the exploration of an open state stabilized by intrastrand contacts.[32]

F-actin binding proteins such as myosins that bind the D-loop near the variable D-loop/C-terminal longitudinal contacts are likely sensitive to the dynamic state of the filament. The Merino et al.[33] and Chou and Pollard[32] studies both agree that loss of P_i in the nucleotide binding site relayed by the sensor-loop (Figure 8b) can increase the dynamics of the D-loop/C-terminal longitudinal contacts as well as the lateral contacts made nearby with the hydrophobic plug. The dynamics within and between the F-actin subunits controls the different twisted states explored by the filament that can be exploited for selective binding of proteins such as cofilin.[43] Thus, F-actin dynamics is an important component at the heart of the selective recognition between young and old filamentous actin. More studies are required to fully understand how allosteric sites control the dynamics in this region. Note also that selection of filaments in class averages for Cryo-EM studies reveal some snapshots of states explored by a filament at higher resolution but these cannot provide direct access to the transient states explored or the dynamics of the filaments. Since myosin motors can develop work under strain when bound to F-actin, studying how motor interactions change the F-actin structure and its dynamics along the cycle is essential.

3.3.2. F-Actin Structure When Myosin Is Bound in Strong-ADP and Rigor States. All actin−myosin structures determined to date at 3.3−4.6 Å best resolution[36,39,95] indicate that the F-actin filament is not twisted upon myosin binding in the Rigor state. The actin side of this interface is similar in these structures,[36,39,95] with some reported minor changes in the Myo6-bound structure (see below). The closed configuration of the D-loop is critical in the hydrophobic core of this complex and is stabilized by strong interactions with the myosin HTH surface, which cannot occur with an open configuration of the D-loop (Figure 8c). Note that no steric clash would however occur between myosin bound to an open configuration of the D-loop.

Overall, minimum differences are found on the actin side when these rigor decorations are compared, and the same F-actin conformation is seen for the Strong-ADP state of Myo1b. Local changes are restricted mainly to the intrinsically disordered N-terminus region that does not always participate in myosin binding and to the C-terminus peptide of F-actin (after residue H371) which is helical and stabilized by intra-subdomain-1 interactions in reconstructions with NM2c and Myo1b but is less ordered in Myo6 decorations. The D-loop seems to adopt in fact a more disordered state when Myo6 binds,[95] which is possibly related to its preference for ADP-bound, less rigid filaments rather than ADP.Pi-bound filaments.[150] The fact that the ADP-bound F-actin structure is conserved among these myosin strong binding states while the decoration is done with or without F-actin stabilizers (Myo1b) may indicate that strong binding of myosin selects the closed D-loop configuration, but more actin−myosin structures are required with the use of jasplakinolide to establish whether the open D-loop is destabilized by myosin binding. In contrast to Myo6, Myo5 not only has a preference for ATP-bound F-actin tracks, but low-resolution Cryo-EM analysis suggested that its Strong-ADP state would induce a different twist in F-actin.[94] Higher-resolution studies of both the Rigor- and Strong-ADP-bound states of Myo5 (with and without jasplakinolide) could provide important further insights on how myosin may influence F-actin in the strong bound states and its relationship with selectivity for some myosins for young versus old F-actin tracks. The current structures indicate, however, that the impact of the myosin motor on its track is minimal in the Rigor state and that twisting of the filament does not occur in this state even upon saturation of the actin binding sites by myosin motors.

Whether myosin induces long-range conformational changes in the actin filament upon populating strongly attached states and whether this is mainly communicated by the thin filament regulation proteins on F-actin in muscle needs more investigation. Cryo-EM structural studies that require saturation of the sites by myosin may interfere with the twist or dynamics of the actin filament and still need higher resolution for investigating how the actin track is influenced by myosin binding. In a physiological context, actin filaments are dynamic, exhibiting different and variable curvatures, and this could be a key component of how myosin lowers energy barriers between the states of the powerstroke. The other dynamic components of the filament such as the D-loop conformation and the N-terminal extension allow the exploration of conformations of F-

DOI: 10.1021/acs.chemrev.9b00264
Chem. Rev. XXXX, XXX, XXX−XXX

actin that are likely also to facilitate the formation and the transitions of the actin−myosin complex.

3.4. Conserved and Variable Features of the Rigor Interface among Different Myosins

The recent Cryo-EM structures of Myo2, Myo1b, and Myo6 allow an overall comparison of the Rigor state of myosins from different classes. The current maps cannot fully describe the interface in atomic detail, since the electron density for the side chains of several residues is missing and the description of hydrogen bonds and water mediated bonds would require higher (<2.5 Å) resolution. Current limitations in resolution may be linked to dynamic transitions among different Rigor states, as previously proposed.[121] The footprint on the filament found from Cryo-EM reconstructions of Myo2 and Myo1b can be used to compare the interface at higher resolution than is possible for Myo6.[95] Interestingly, some common and different features among these Rigor structures are clearly revealed by the current maps, as described below.

3.4.1. Conservation and Variability in the Footprint of Myosin Binding on F-Actin. The footprint of the motor in Rigor states corresponds to the actin residues involved in interaction with myosin. In the three actin−myosin interfaces, a large part of the binding energy seems to be provided by apolar patches that occupy similar sites on the F-actin surface in the center of the interface. Thus, in spite of differences in sequence of their actin binding elements, NM2c, Myo1b, and Myo6 have a similar surface topology of hydrophobic and charged (or polar) patches that allows them to bind actin in a similar way: the apolar or negatively charged surface of the ^{L50}HTH avoids the two negatively charged surfaces found in subdomain-1 of both Actin-1 and Actin-2 and occupies a more positively charged surface that corresponds to the C-ter/D-loop interface between these two subunits of the filament.

As shown in Figure 9, the footprint is quite similar for Myo1b and NM2c. Most of the actin residues involved in binding the HTH and HCM-loop at the center of the interface are conserved in these high-affinity actin−myosin interfaces with differences in sequence for the turn of the HTH leading to only local adaptations of the contacts with F-actin. Differences in the peripheral sites of the footprint are due to the large structural differences of more variable loops of the $_{M}$ABS such as (i) Loop2 and the HW helix for which electron density supports interaction for Myo2 with the flexible N-terminal region of F-actin, but not for either Myo6 or Myo1b; (ii) in contrast, Loop3 and Loop4 make more contacts in the case of Myo1b than NM2c (Figure 9). However, the footprint and overall orientation of these two motors on F-actin are quite similar (Figure 10a,c). In the NM2c Rigor structure, tropomyosin occupies a site adjacent to where Loop4 binds. In fact, tropomyosin covers residues that are found to interact with Loop4 of Myo1b (Figure 9). The presence of tropomyosin can thus influence the affinity of strong binding states of different myosins, and this explains the selectivity of Myo1b for filaments deprived of tropomyosin.[153,154]

The footprint of Myo6 on actin, in contrast, differs significantly from those of Myo1b and NM2c (Figure 9). While the central core residues of the footprint that interact with the ^{L50}HTH and ^{U50}HCM-loop are similar, the contacts they make differ in detail. It is noteworthy that the closure of the internal cleft is similar for the three Rigor structures solved to date at high resolution. In fact, no major differences are found in the internal conformation these motors adopt upon

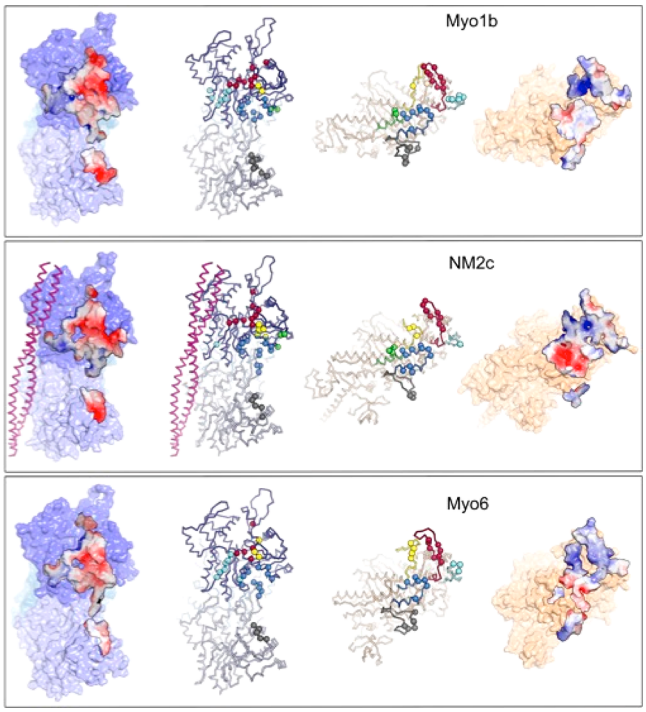

Figure 9. Comparison of three actin−myosin interfaces in strongly bound states. Cryo-EM structures of Myo1b (Strong-ADP, PDB ID 6C1G, EMD7330[39]), NM2c (Rigor, PDB ID 5JLH, EMD8164[36]), and Myo6 (Rigor, PDB ID 6BNP, EMD7116[95]) are compared. The labeling and color scheme are the same as those in Figure 7b,c: Loop4 in cyan; HCM-loop in red; Loop2 in yellow; helix-turn-helix (HTH) in marine blue; activation loop in green; Loop3 in gray.

forming the strong binding interface (Figure 6a). The differences in the footprint between these Rigor structures are linked to differences in the positioning of these two motors on F-actin, which is not determined by conserved interactions at the center of the interface (Figure 10b,d,e). The overall positioning of the motor seems to be, in fact, greatly influenced by peripheral loops. Thus, several contacts involve ^{U50}Loop4 and ^{L50}Loop3 in the Myo6 Rigor density, while they are more limited in the case of NM2c and Myo1b. The Activation-loop is not involved in interaction with F-actin in the Myo6 rigor interface, in contrast to what is found for NM2c and Myo1b. In Myo6, the ^{U50}HCM-loop is larger and the tip of the loop seems to explore some disorder, although some contacts may extend the footprint on F-actin (Figure 9). The interface is thus the sum of contacts that can occur by globally positioning the motor such that core hydrophobic interactions (of similar but not identical nature) can take place while other peripheral sites modulate the global interaction. The distinct class-specific differences in the exact nature of the interactions between the motor and the actin filament indicate that interactions of the motor with the track must result from global recognition of the actin interface rather than a specific set of conserved contacts. The actin binding surface of the motor is thus likely to play an important role in tuning each motor's activity as it interacts with its track.

3.4.2. Overall Positioning of Myosin on F-Actin in the Rigor Structures. The analysis of the NM2c, Myo1b, and Myo6 rigor interfaces shows that the variability and adaptability of the actin binding surface make it impossible to predict how the different loop components will influence the precise orientation of the head and the interactions that can

DOI: 10.1021/acs.chemrev.9b00264
Chem. Rev. XXXX, XXX, XXX−XXX

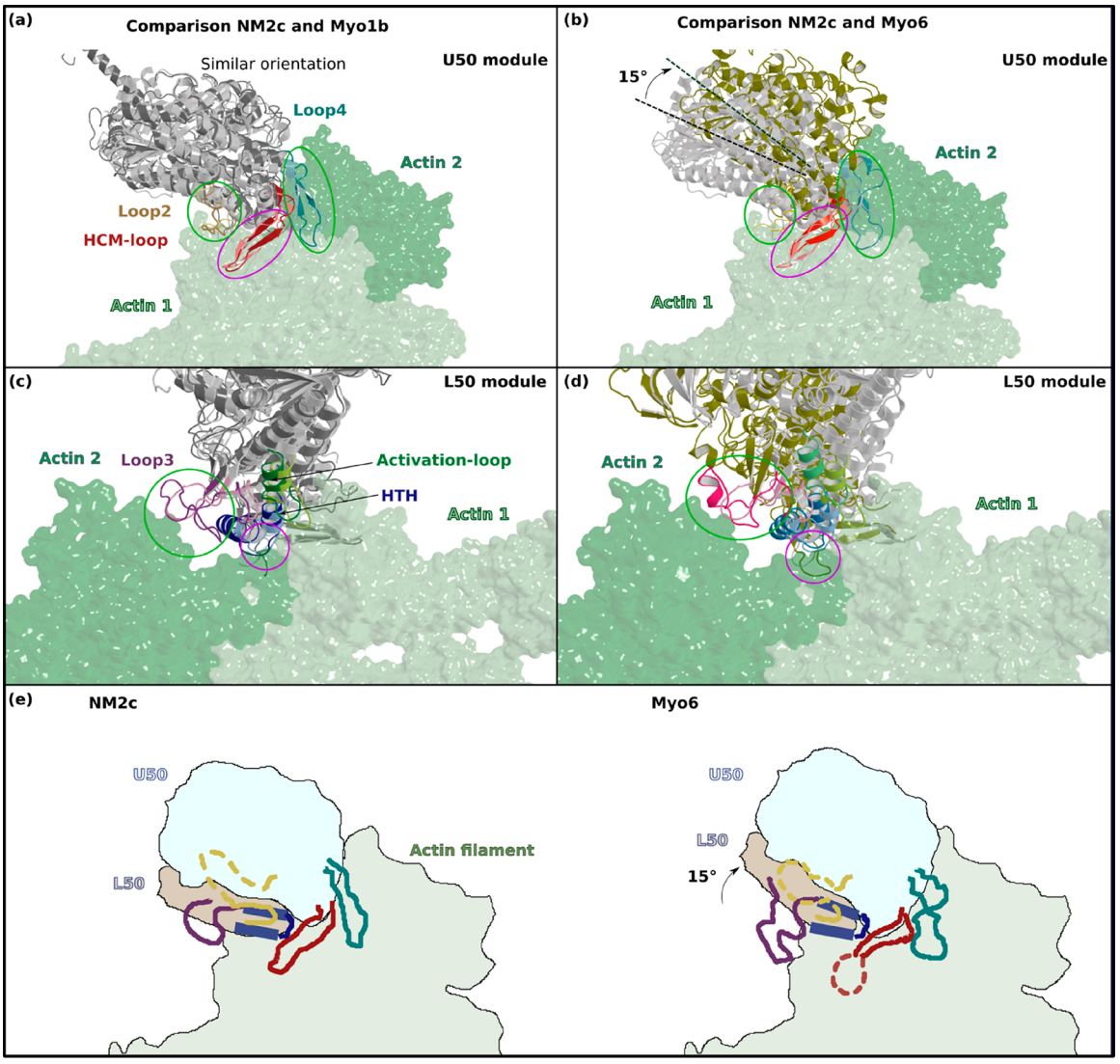

Figure 10. Overall positioning of the motor on F-actin in different Rigor actin−myosin structures. In parts a and c, NM2c (Rigor, PDB ID 5JLH, EMD8164[36]) and Myo1b (Rigor, PDB ID 6C1H, EMD7331[39]) are compared; in parts b and d, NM2c and Myo6 (Rigor, PDB ID 6BNP, EMD7116[95]) are compared. Panels a and b, view of the U50 module (HCM-loop, Loop4, and Loop2) bound to F-actin. Panels c and d, view of the L50 module (HTH, Activation-loop, and Loop3) bound to F-actin. Note that the NM2c and Myo1b are bound to F-actin with a similar orientation. In contrast, the orientation of Myo6 differs by ∼15° from that of NM2c. The conserved actin binding elements are circled in magenta, while the variable ones are circled in green. (e) Schematic and simplified diagrams of the NM2c and Myo6 actin binding elements, as well as their anchoring from their relative subdomain. Note how these actin binding elements differ both in length and in orientation. Note also the orientation of the motor on the F-actin track that differs by 15°.

occur upon F-actin binding in the Rigor state for different myosin motors. The two major components of this interface, the ^{L50}HTH- and ^{U50}HCM-loops, find similar sites on F-actin but interact differently in detail. The use of the flexibility at the anchoring points of the HCM-loop and Loop4 allows them to find similar sites on the actin surface for different myosins without imposing in fact the same orientation for the whole motor on the track (Figure 10b,d,e).

This allows different contacts from Loop2, the Activation-loop, and Loop3 to influence and modulate the interaction, since their sequences greatly vary among rigor complexes. Since prediction of Rigor structures is not possible, more structures should be solved to complete this small set and define how the strong binding states may vary among different myosin motors. The change in orientation of the head among Rigor structures does not however impact greatly the lever arm position: in all Rigor states, the Converter adopts a down position that does not vary significantly with the change in overall orientation of the motor on actin. In fact, more than the overall change in orientation described here and which impacts the contacts made at the interface, the position of the lever arm in Rigor is influenced by the contacts made with other elements of the motor found in N-terminal extensions or the N-terminal subdomain.[39]

Thus, a remarkable feature of these Rigor structures is the fact that the motor domain itself conserves a similar conformation at the end of the powerstroke, when no nucleotide is bound. This suggests that the motor rearrangements (exact inner cleft closure in Rigor, changes in transducer defining the general position of the connectors in the motor) are specified and constrained by the binding to F-actin. The rate of the transitions between the states explored during the

DOI: 10.1021/acs.chemrev.9b00264
Chem. Rev. XXXX, XXX, XXX−XXX

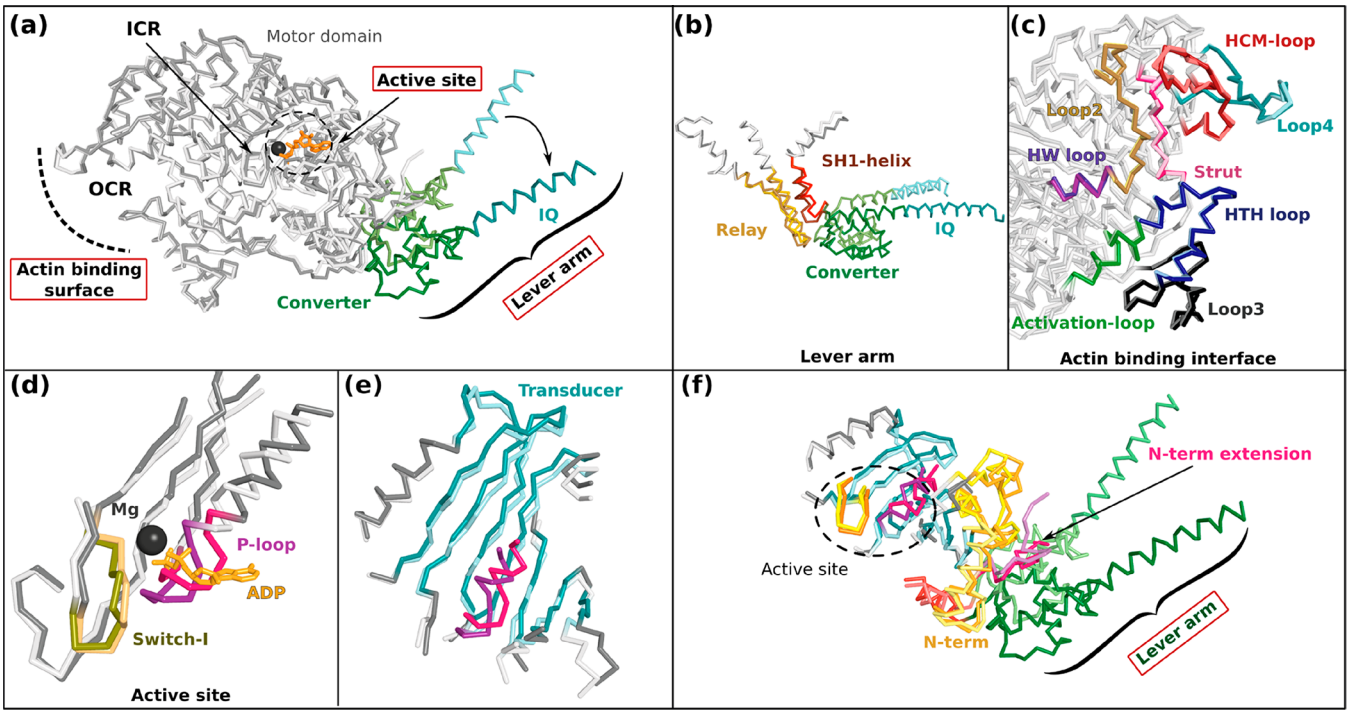

Figure 11. Conformational changes upon ADP release, last step of the powerstroke. Comparison between the Myo1b (Rigor, PDB ID 6C1H, EMD7331) and Strong-ADP (PDB ID 6C1D, EMD7329) states[39] superimposed on both the U50 and L50 subdomains. To differentiate the two states, a color gradient is used in all panels and for all the elements, with the Strong-ADP state features displayed with lighter colors and the Rigor state with darker colors. (a) Overview illustrating the difference in lever arm orientation between the two states. (b) View of the connectors driving the lever arm orientation: SH1-helix (red) and Relay (yellow). (c) View of the actin binding interface ($_{M}$ABS): HCM-loop, red; Loop4, cyan; Strut, pink; Loop2, yellow; HO-helix, purple; HTH, blue; Loop3, black; Activation-loop, green. (d) Active site: P-loop (purple for Strong-ADP, hot pink for Rigor) and Switch-I (yellow for Strong-ADP and olive for Rigor). Tight coordination of MgADP by both the P-loop and Switch-I cannot occur in Rigor. (e) Representation of the central β-sheet in the motor (which is part of the transducer) near the active site (P-loop, purple/hot pink). (f) Overall view of the Myo1b connectors and the N-terminal extension (light pink/hot pink). Note the reorientation of the N-terminal subdomain (yellow, Strong-ADP; light orange, Rigor). In the Rigor state, the N-terminal extension (hot pink) can dock between the motor domain and the Converter, but this is not possible for the Strong-ADP state.

powerstroke can greatly vary among myosins, since it is dependent on the interactions F-actin can make with these different states and thus the composition of the myosin surface at the actin interface, as well as the strain developed within the structural elements of the myosin motor domain.

3.5. The Last Step of the Powerstroke: ADP Release

ADP release while the myosin motor is strongly bound to F-actin corresponds to the last step of the powerstroke. It is a key transition to regulate the motor function, since, for several unconventional myosins, it controls the duty ratio and thus the amount of time the motor spends bound to F-actin along its cycle. For high-duty-ratio motors, such as processive motors or strain sensors, this is the slowest transition in the overall cycle.[3,13,14] In addition, load-sensitive motors can stay attached to F-actin with MgADP bound for a long period of time even when high reversal force is exerted on the motor. A slow ADP release rate might not always translate into a high duty ratio, since entry into the force-generating states could also be slow. Such is the case for non-muscle myosin IIb.[89]

In the Rigor state, Mg^{2+} cannot bind strongly and thus ADP release is facilitated in this state.[62,83,94,126,127] The actin–myosin state that precedes Rigor in the cycle is called the Strong-ADP state and has a strong affinity for both Mg^{2+} and ADP. As first visualized with Cryo-EM[78,93] and also detected in optical trap studies,[81] the transition between Strong-ADP and Rigor is accompanied by a lever arm movement (Figure 11a,b).

Higher-resolution studies[39,94] have indicated that the actin binding interface in the Strong-ADP state does not differ from the Rigor state in a significant manner (Figure 11c), consistent with lack of effect in the kinetics of this last step of the powerstroke dependent on mutations in loop2 or the HTH surface.[155,156] However, one cannot exclude at the current resolution that the interfaces differ for local conformations or for the dynamics of the $_{M}$ABS. This question remains open until atomic resolution (complete side chain interaction description) will be provided. The release of Mg^{2+} followed by ADP is controlled by the isomerization between Strong-ADP and Rigor.[83,126,127] Cryo-EM studies at ~7.6 Å resolution,[94] confirmed, as did studies of two other motors at higher resolution,[39,95] that a movement of the P-loop relative to Switch-I is the basis of this loss of ADP from the active site[83] (Figure 11d). This movement is linked to an internal isomerization of the motor related to conformational changes in the transducer[39,94,95] (Figure 11e). Variations in the loop1 sequence (Figure 3c), which belongs to the transducer, have indeed been reported to tune ADP release for several myosins.[139,157,158] The transducer changes are amplified by a large movement of the N-terminal subdomain (Figure 11f) and are coupled with the SH1-helix and Relay movements that guide the Converter position (Figure 11b,f).

The differences between Strong-ADP and Rigor can lead to drastic changes at the interface between the Converter and the rest of the motor domain linked to a difference in the lever arm

DOI: 10.1021/acs.chemrev.9b00264
Chem. Rev. XXXX, XXX, XXX−XXX

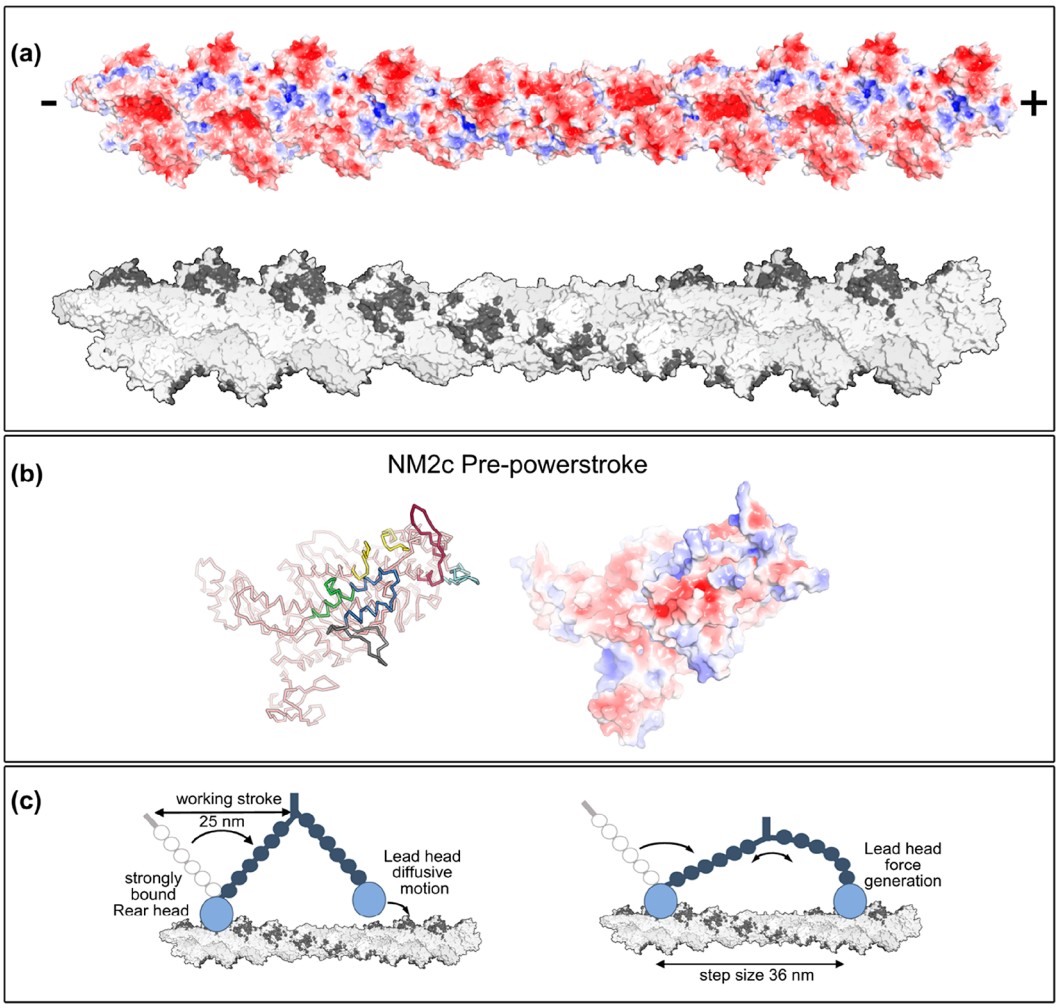

Figure 12. Distribution of the myosin binding sites on F-actin. (a) Top, F-actin surface colored by electrostatic potential distribution (red −5; blue 5 K_bT/e_c). Bottom, Myosin binding sites (dark gray) are mapped on the actin filament (light gray). (b) NM2c in the Pre-powerstroke conformation (PDB ID 5I4E[66]). Left, the actin binding elements are colored as in Figure 7. Right, the NM2c surface is colored according to the electrostatic potential distribution (red −5; blue 5 K_bT/e_c). (c) Schematic drawing of two-headed Myosin V walking along F-actin. The length and flexibility of the lever arm and head/head junction permit lead head diffusion to the most favorable actin binding sites on the track.

position. In Myo1b, this leads to the ability for the N-terminal extension to stabilize the Rigor conformation, in which it can dock (Figure 11f, hot pink), whereas this N-terminal extension is flexible and undocked in the Strong-ADP state (Figure 11f, light pink). Another way for the N-terminal extension to stabilize the Rigor state has been visualized for PfMyoA myosin. In this case, phosphorylation of a serine in the N-terminal extension stabilizes the Rigor state by interaction with a lysine of the Converter. In this myosin, a phosphorylation event changes the duty ratio and may thus allow the motor to be tuned for different cellular roles depending on the stage of the parasite.[46]

For the ADP release step of the powerstroke, sequence differences among myosins located in the actin binding interface are thus unlikely to be as important as those in the motor itself, in particular those found in the transducer. In addition, the Myo1b and PfMyoA demonstrate that N-terminal extensions are key elements to tune this transition. This is an essential step for myosins to modulate under load so that they can be optimized for processive movements, for fast sliding of filaments, or for force-sensitive anchoring.[3,13,14,159]

4. FORCE GENERATION AND TRANSITIONS DURING THE POWERSTROKE

4.1. How Myosin Finds Its Docking Site on F-Actin and Engages in Force-Producing States on the Track

F-actin is a periodic negatively charged filament (Figure 12a). The rigor footprint described earlier contains a hydrophobic, poorly charged region (D-loop/C-ter surface) adjacent to a negatively charged region (centered on Actin-1 subdomain-1) (Figure 9). On the myosin side (Figure 12b), several actin binding loops are positively charged. Earlier studies with Myo2 have shown that the initial complex largely involves charge−charge interactions, followed by two large conformational changes guided by the formation of stereospecific hydrophobic interactions, and sensed simultaneously by fluorescent probes on F-actin and myosin.[91,92] The first stereospecific actin−myosin complex is followed by formation of a stronger binding complex in which the interface formed is similar to that of the Rigor state. Early work is consistent with this transition involving cleft closure, as of the isomerization rate is pressure-sensitive, suggesting that a significant conformational change of the actin−myosin subfragment-1 complex[148] occurs that

DOI: 10.1021/acs.chemrev.9b00264
Chem. Rev. XXXX, XXX, XXX−XXX

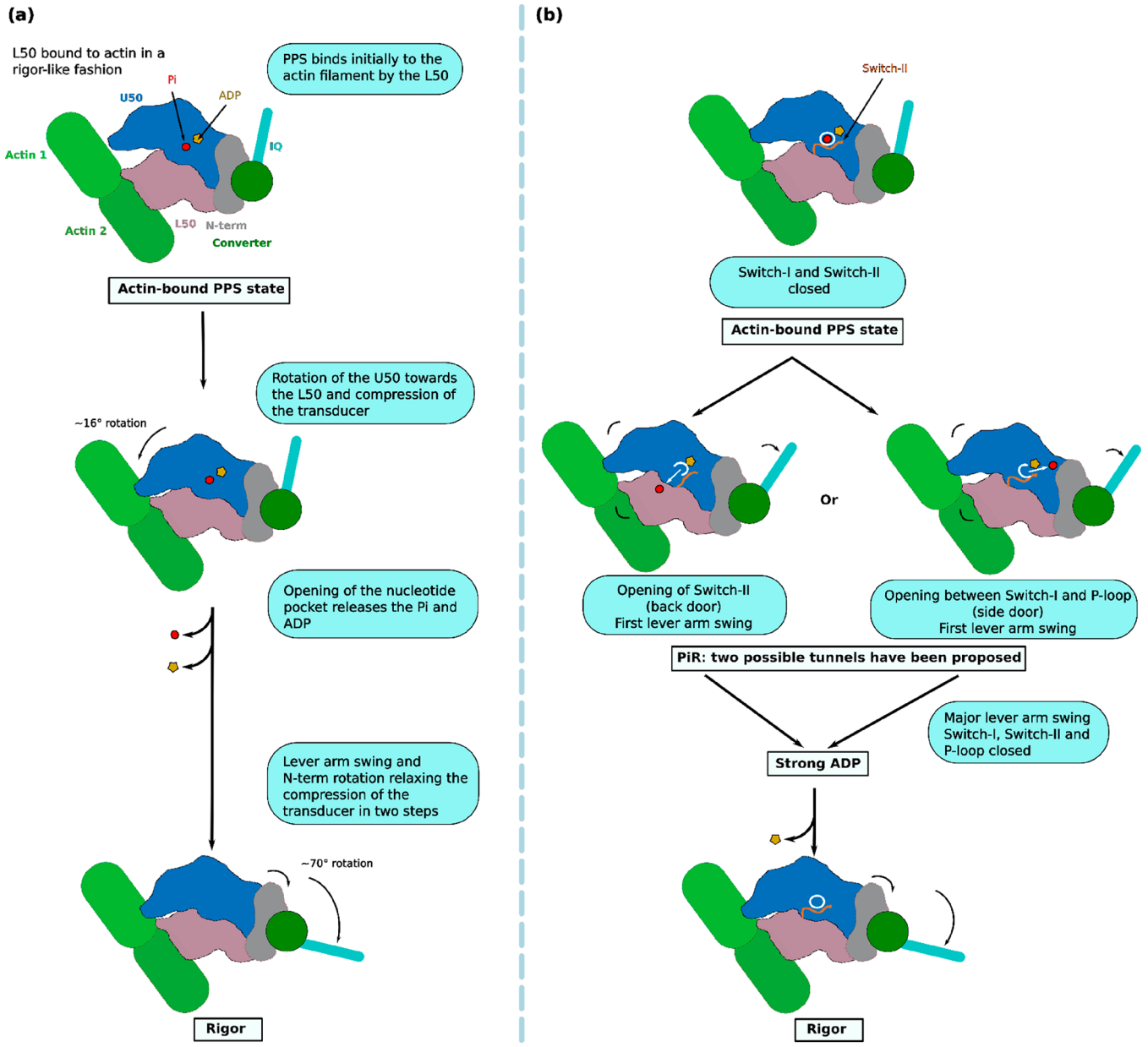

Figure 13. Different models of cleft closure during the powerstroke. (a) Schematic representation of the model proposed by Behrmann and co-workers.[121] Docking of the L50 subdomain of the Pre-powerstroke to F-actin was proposed to occur to create some of the rigor interface. The full rigor interface was then proposed to form via cleft closure (by a 16° rotation of the U50 subdomain), creating a state in which strain would build in the transducer and the N-term subdomain. Relaxation after release of P_i was proposed to swing the lever arm by rotation of the N-term subdomain and untwisting of the transducer. Preller and Holmes proposed a similar model[170], although in this case a 16° rotation of the L50 subdomain was proposed to induce the formation of a hypothetical state (the Start-of-Power Stroke) with a fully closed cleft and a lever arm primed. (b) An intermediate must occur to allow P_i release prior to full cleft closure, as demonstrated by functional experiments.[60] Historically, two alternative possible paths were proposed for P_i release: the back door and the side door mechanisms.[60]

involves displacement of a large amount of water from the interface and/or the internal myosin cleft.[58] EM studies with regulated thin filaments[160,161] indicated that some of the contact sites of Actin-1 subdomain-3 are covered by tropomyosin in the absence of myosin but are involved with myosin in the strong rigor interface. This indicates that, for Myo2, the initial complex likely involves mainly Actin-1 subdomain-1 and/or the D-loop/Cter intersubunit surface.

Electrostatic interactions greatly influence the first stereo-specific binding of myosin to actin.[155,156,162,163] Myosin may explore the actin surface guided by electrostatic steering, avoiding repulsive interactions. These encounters may not all always trigger entry of the myosin into force productive states, instead allowing diffusion along the track without consumption of ATP.[164] For processive motors such as Myo5, which has a stroke size of 25 nm (Figure 12c), the periodicity of the filament guides the step size between the rear and the lead head: the attachment of the motor by the rear head allows the lead head to explore, using Brownian motion, a number of actin binding sites favoring reattachment at 36 nm, corresponding to the helical periodicity of the filament.[165]

DOI: 10.1021/acs.chemrev.9b00264
Chem. Rev. XXXX, XXX, XXX−XXX

4.2. How F-Actin Directs Force Generation by Myosin during the Powerstroke

Functional studies have accumulated evidence for the role of dynamics within the actin−myosin complex for more than 30 years. These transitions are directly linked to the interplay in the motor between events at the three allosteric sensing sites that control release of hydrolysis products depending on events triggered by F-actin and that are also connected for some of the transitions to a lever arm movement. Kinetic studies for distinct myosins have detected similar transitions, although at different rates.[6,13,14] It is possible, however, that there are critical events that have not been measured distinctly by the current kinetic studies.

For force generation to occur in a productive way, formation of the actin−myosin complex must be rectified (engaged in a strong binding state from which dissociation is faster if force is applied in one direction compared to the opposite one), prior to the loss of P_i or the swing of the lever arm. A strong binding interface must form early in the powerstroke in order to prevent detachment from F-actin. In addition, functional studies[166−168] have shown that load (opposing force) is required for the motor to be sensitive to P_i. Since P_i rebinding requires the reversal of load-sensitive steps), the lever arm swing must be coupled with the closure of P_i access to the active site. Recent optical trap studies have also shown that early states of the actin−myosin complex that detach at fast or intermediate rates are the only ones sensitive to 10 mM P_i.[169] Thus, the early events of the powerstroke must allow the motor to be engaged in a force-bearing attachment to F-actin that allows P_i release, followed by conformational changes that drive the major component of the lever arm swing and prevent Pi re-entry. Below, we review the structural and functional data that have provided insights in the force development transitions of the motor cycle.

4.2.1. Early Concepts and a Simple Model for the Powerstroke Events on F-Actin. The kinetic transitions detected for the powerstroke were first interpreted with simple hypothetical structural models[121,170] (Figure 13a) based on (i) what was known then about weak and strong actin binding states (Figure 4c) and (ii) the assumption that increase in affinity for the complex would be based on forming some of the contacts of the final rigor complex, while motor conformational changes would allow the progressive formation of more individual contacts, keeping those formed earlier to avoid detachment of the motor. These earlier models proposed that the formation of the rigor interface by full closure of the inner cleft would precede the lever arm swing, causing the formation of internal strain in the motor that would be released upon lever arm movement[170] (Figure 13a). Docking of the Pre-powerstroke state via the formation of some of the contacts found in Rigor (L50 subdomain[121] or U50 subdomain[170]) was proposed to induce formation of a hypothetical strained state (Start-of-Power Stroke) **prior to P_i release**, with a fully formed rigor interface (inner cleft closed) and that would have kept the lever arm primed[121,170] (Figure 13a). This model was disproven however by subsequent studies introducing bulky residues in the outer cleft.[60]

In addition, a major conceptual difficulty unresolved at the time was to explain the mechanism that would allow the release of P_i while keeping the MgADP firmly coordinated in the active site. It became clear at that time that understanding this key event (P_i release) was a central issue to account for the early events of the powerstroke. Two possible paths for P_i release had been proposed to open the active site: either by moving Switch-II (back door[90,171]) or by creating a gap between the P-loop and Switch-I upon transducer rearrangements that would create an intermediate state along the movement of the transducer required to close the inner cleft (side door[124]) (Figure 13b).

4.2.2. Current Evidence for the Mechanism of P_i Release by Myosin Motors. A crystal structure of Myo6[60] provided new insights into the states the motor can explore and drastically changed the concepts of how the three allosteric sites communicate. In this structure, a new actin interface is formed that differs from both the weak (PPS) and strong (Strong-ADP, Rigor) binding interfaces (Figure 14a). In this new Myo6 structure, a large Switch-II movement opens a tunnel in the inner cleft (back door) (Figure 14b). Experiments where these crystals were soaked in phosphate buffers revealed that P_i can bind stably at the mouth of the tunnel or can move back to the nucleotide binding pocket, where it can induce the reverse isomerization and recreate the Pre-powerstroke state.[60] Functional studies with mutations in the tunnel also established that the mechanism for P_i release in early states of the powerstroke would correspond to the engagement of the P_i in this tunnel and its liganding in a different site at the end of the tunnel nearer the surface of the molecule[60] (Figures 14b and 15).

We have thus proposed that this novel structural state seen at high resolution for Myo6[60] corresponds in fact to the state that binds stereospecifically to actin to initiate force generation and the powerstroke. The structure describes the mechanism that allows actin to activate the release of P_i from the myosin active site. The formation of a new actin interface would destabilize the Pre-powerstroke state in which the P_i is trapped by involving a large Switch-II movement that opens a back door,[60] as previously hypothesized.[90] This state was thus referred to as the Phosphate Release state (P_iR state).

The P_iR structure demonstrated that previously proposed mechanisms for the powerstroke[121,170] were too simplistic, since they had been based on assuming that movements of Switch-II would be directly coupled with a large lever arm swing.[121,170,172] The P_iR structure indicated in fact that only a small movement of the lever arm would occur upon the large Switch-II movement required to open the P_i release tunnel (Figures 14b and 15a) and that this occurred while a different actin binding interface was created (Figure 14a). Functional studies confirmed that introduction of a bulky residue in the outer cleft (OCR) (Figure 3a,b) did not impair the rate of P_i release, confirming that full closure of the cleft is not required for this step.[60] In fact, P_i departure from the site where it is generated in the active site is likely required for complete cleft closure (Figure 15b). The transition in which cleft closure fully occurs is thought to be sensed by pyrene−actin quenching and coupled to some component of the lever arm swing[60] (Figure 16). Thus, opening of the tunnel and departure of P_i from the active site acts as a gating event, ensuring commitment of the motor to the track but preventing lever arm swing until the P_i has reached the surface site at the end of the tunnel.[60]

4.2.3. Plasticity of the Myosin Actin Binding Interface Is Key for Driving the Powerstroke. Based on the studies that elucidated the structural changes required for P_i release,[60] it became clear that several actin−myosin interfaces can occur. Exploration of several conformations of the actin binding loops via their dynamic and different states of the inner cleft can

DOI: 10.1021/acs.chemrev.9b00264
Chem. Rev. XXXX, XXX, XXX−XXX

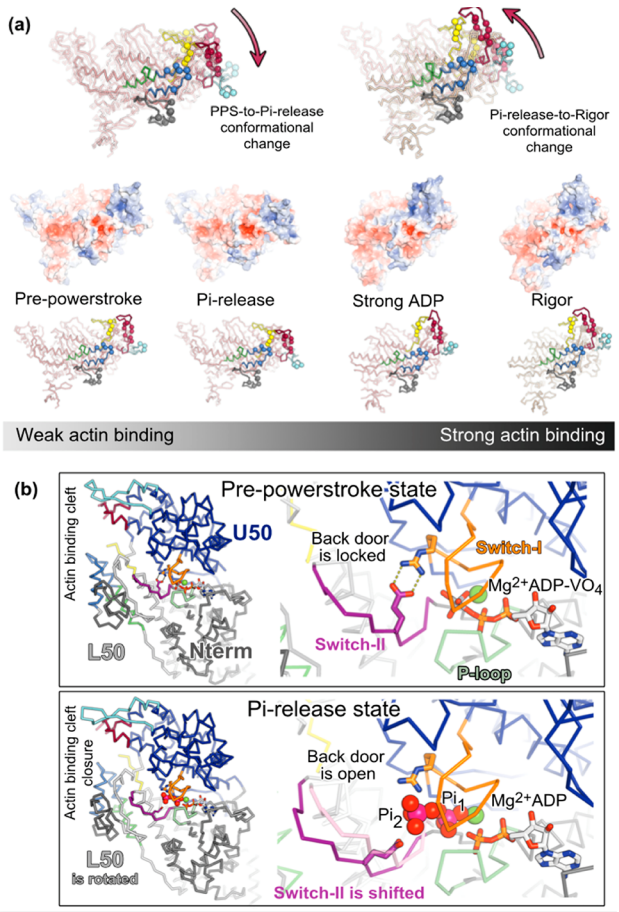

Figure 14. P_i release state, cleft closure, and powerstroke. (a) Myo6 actin binding surface changes during the powerstroke, as mapped with four Myo6 structures: Pre-powerstroke (PDB ID 2V26[111]), PiR (PDB ID 4PFO[60]), Strong-ADP (PDB ID 6BNQ[95]), and Rigor (PDB ID 6BNP[95]). The representation and color scheme are the same as those of Figure 7c. Top, the difference in cleft closure between these states is shown by superimposing the L50 subdomains. Below, the different states are represented as they are populated along the powerstroke. The Myo6 surfaces are shown colored by electrostatic potential distribution (red −5; blue 5 K_bT/e_c). (b) Upper part, Myo6 in Pre-powerstroke state (PDB ID 2V26[111]). (Right) The close-up view of the nucleotide binding site. Switch-I and Switch-II are stabilized by a salt bridge between an arginine (Switch-I) and glutamate (Switch-II) residues that are conserved in all myosins, locking the myosin "back door". Lower part, Myo6 in the P_iR state (PDB IDs 4PJN[60] and 4PJM[60]). Switch-II is displaced compared to the Pre-powerstroke state, opening the phosphate release tunnel at the back door. Two phosphate sites (red balls) can be occupied, as observed in the crystal structures upon soaking experiments.

favor transitions to produce stronger binding interfaces with the track coupled to the powerstroke. Our current vision of how the interface adapts to keep the motor engaged and progressively favors rearrangements in the motor permitting the release of P_i from the active site and the lever arm swing is based on the plasticity of the actin−myosin interface described earlier in the comparison of different rigor complexes (see section 3.4).

Since the rigor interfaces of different myosins can differ in the detailed contacts they form and in the overall orientation of the head to the F-actin track, we propose a model in which exploration of actin by the myosin surface available for interaction with the track (including possible influence from peripheral actin binding loops) would guide the interactions made by each of the sequential powerstroke states with the track, rather than a very strict and conserved set of interactions that all myosins would have conserved to promote these transitions. It is thus likely that the exact contacts made to stabilize the P_iR state attachment to the F-actin track are not all conserved with those that have been described for the strong binding states of a particular myosin.

For the first transition that allows the stabilization of the P_iR state, functional studies of mutants have revealed features that are conserved among myosins that favor this transition.[60] Such studies have revealed the importance of the positively charged residues of Loop2[155,156,162] and the Activation-loop[60,163] as well as the charge and hydrophobic residues of the ^{L50}HTH turn[156,173] to form and stabilize the first stereospecific binding interface. In contrast, the ^{U50}HCM-loop may not play a major role in this first transition, while it would be critical to drive formation of the stronger binding states in which the inner cleft is closed.[36,60,173] It is interesting to note that the Activation-loop plays a major role in Myo6 for the transition toward the P_iR state,[60] while it is not part of the rigor interface.[95] This illustrates the point that all contacts created early are not kept along the transitions of the powerstroke. We are currently lacking a visualization of the actin−myosin complex in these early states of the powerstroke, which would precisely describe the interactions that engage the motor in force-producing states.

4.3. Force Production Is a Multistep Event Triggered by Actin Binding

Recent functional studies and the structures available to date allow us to propose a model of force generation that can account for the published findings. The challenge for the structural data has been to properly associate the structures with their place in the functional cycle. The proposed P_iR structure is possibly the most debated, because of seeming discrepancies with functional studies,[61] some interpreted as indicating P_i release occurs prior to the lever arm swing[60,174−176] and others interpreted as indicating that P_i release can only occur after the lever arm swing.[167,169,177−180] However, as we outline below, we think that all of the current multidisciplinary data are in agreement and can be accommodated in one unifying model for force generation (Figure 16). An important piece of evidence supporting the model comes from a surprising source, namely, from the development of a drug that enhances force generation in the heart, omecamtiv mecarbil (OM).[21,22]

Force generation is initiated when myosin binds to actin with a stereospecific interaction. Prior to this, the myosin motor domain can interact weakly and non-stereospecifically with actin in the Pre-powerstroke state via electrostatic interactions provided by the flexible surface loops of myosin. The loops themselves are variable among myosin classes, and this may allow selectivity for the actin track[153,154] as well as optimization of electrostatic steering that is required to position the myosin head for rapid formation of a stereo-specific interaction with actin. Note that the presentation of the myosin head to an actin filament will vary depending upon constraints imposed either by a myosin filament (class II myosins) or by the myosin lever arm which, in conjunction with the structure of the actin filament, specifies the optimal reachable actin binding sites[96−99,102] (Figure 12c).

DOI: 10.1021/acs.chemrev.9b00264
Chem. Rev. XXXX, XXX, XXX−XXX

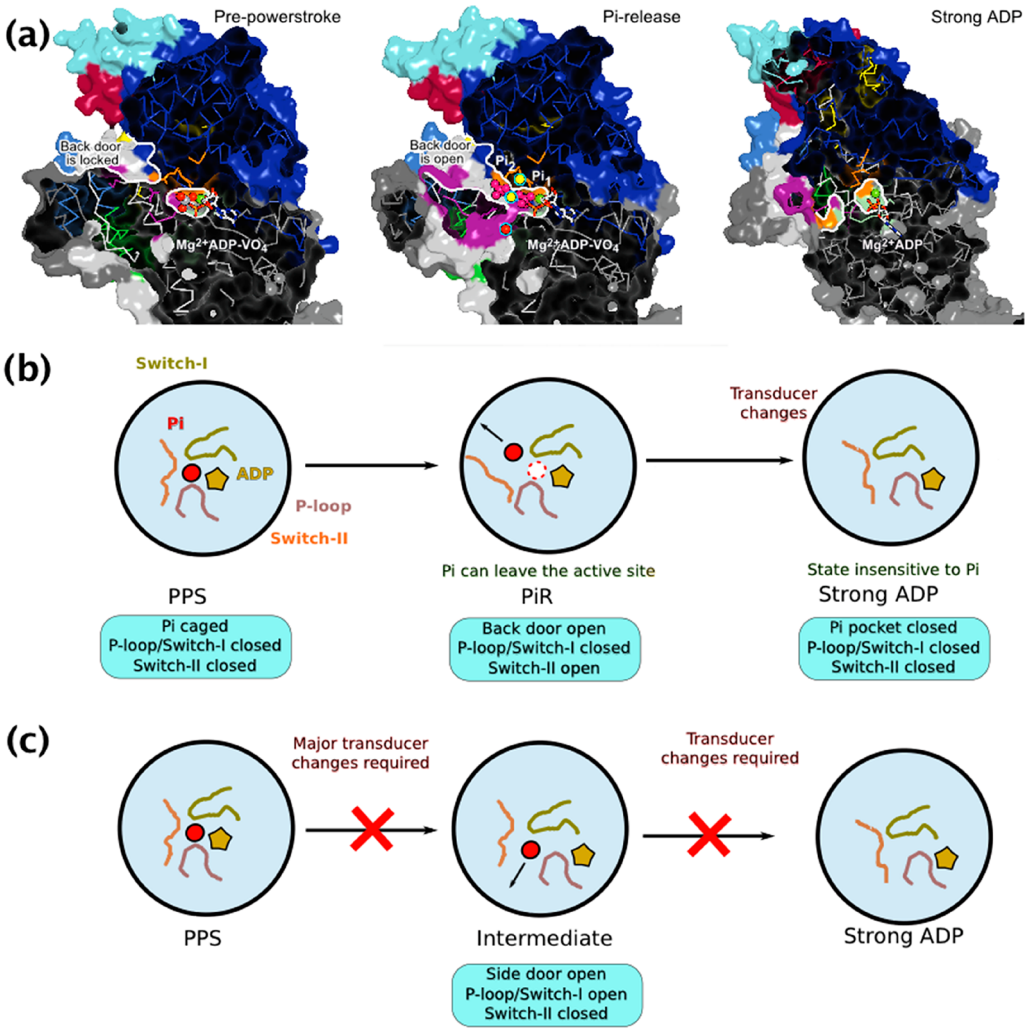

Figure 15. Tunnel for P_i release state. (a) Myo6 is shown in the PPS (left, PDB 2V26[111]), P_iR (center, PDB 4PJN[60] and 4PJM[60]), and Strong-ADP (PDB 6C1D[39]) states in surface representation. The front part of the molecule is cut to illustrate the P_i tunnel connecting the active site with the protein surface. A tunnel for P_i release is open in the P_iR, while the active site is closed in the other two structural states. In the P_iR state, the yellow circles correspond to the location of mutant side chains along the back door that have an effect on the rate of P_i release,[60] while the red circles correspond to the side chain of the side door E152A mutation, which does not change the P_i release rate, although it slows down the following rate monitored by pyrene-quenching.[60] (b) The changes of the nucleotide binding elements required for the backdoor mechanism are shown based on these Myo6 structures. (c) The side door mechanism requires an intermediate in which movements of the nucleotide binding elements are achieved by a relative movement between P-loop and Switch-I linked to transducer rearrangements. This pathway is unlikely, as the presence of P_i would greatly increase the energy barrier required for the transducer transition required to separate Switch-I and P-loop.

From the Pre-powerstroke state, the actin track can induce a transition from a weak binding to stereospecifically engaged interactions with the track (i, in Figure 16). In particular, the ^{L50}Activation-loop (Figure 3) appears to be important in positioning the L50 subdomain of myosin on actin[60,163] to induce the transition to the P_iR state, which involves a translocation of the L50 subdomain (relative to the U50 subdomain) coupled to a rearrangement of Switch-II (Figure 16). These actin binding induced changes create a tunnel that opens an escape route for P_i to move from the nucleotide binding pocket into the second site at the mouth of the tunnel nearer the solvent (Figure 14b). Thus, the transition to the P_iR state involving a conformational change in the motor can be sensed prior to the release of P_i into solution, since P_i may be transiently retained by coordination at this second site. Force is initiated by this isomerization that provides stereospecific actin binding. Force is further developed by the motor in the next transition (ii, in Figure 16) that requires P_i departure from the active site and translocation to the end of the tunnel. Departure of P_i from the active site is required to lower the energy barrier for the transition to the myosin states of increased actin affinity, since these states are not compatible with P_i being bound within the inner cleft at the distal end of the tunnel (near ADP). (In essence, phosphate "wedges" the cleft open.)

Following this initial, stereospecific binding to actin and departure of P_i from its proximal site, a rapid rearrangement of the myosin interface is achieved by closing of the large internal cleft in the motor domain, which is coupled to a swing of the myosin lever arm (ii, Figure 16). This provides both gating and rectification of the actin−myosin interaction. It provides gating by the cleft closure preventing the return of P_i to the nucleotide binding pocket (disruption of the P_i release tunnel). Thus, P_i is released into solution once the rapid closure of the cleft and lever arm swing occurs. This point was not fully appreciated until probes on the lever arm[177,178] revealed that

DOI: 10.1021/acs.chemrev.9b00264
Chem. Rev. XXXX, XXX, XXX−XXX

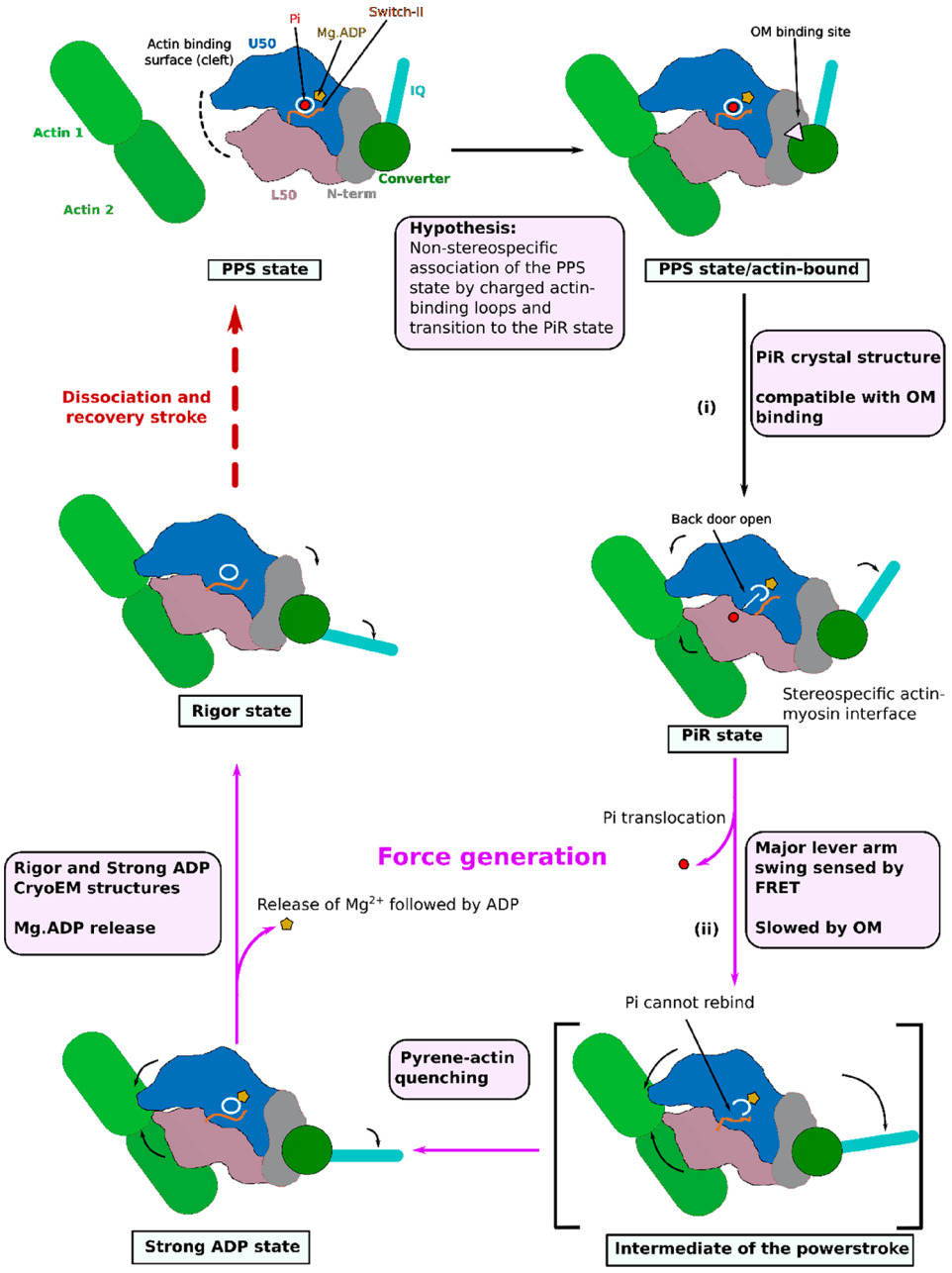

Figure 16. Force-generating cycle. Schematic representation of the unifying multistep force-generating cycle proposed on the basis of recent multidisciplinary results. According to this model, electrostatic interactions between charged actin binding loops (in particular Loop2 and HCM-loop) form non-stereospecific association of the myosin Pre-powerstroke (PPS) state and F-actin. This first association by elements from both the U50 and L50 subdomains induces a first conformational change in myosin that changes the closure of the cleft in the outer cleft region (OCR) and opens the cleft in the inner cleft region (ICR), which creates an escape route (tunnel) for the P_i at the active site. The P_iR state, thus formed, is stabilized on F-actin, since it differs from the PPS state by a new actin binding surface that can dock stereospecifically, creating bonds with F-actin via the ^{L50}HTH and the Activation-loop. In the P_iR state, the P_i release channel opens via opening of Switch-II, allowing P_i to escape from the active site. Release of the ion into the solvent might however be slowed, since it can occupy another site at the end of the P_i release tunnel.[60] The departure of the P_i from its position (next to ADP) in the active site lowers the energy barrier required to fully close the inner cleft. Stronger interactions with F-actin on either side of the cleft stabilize a new conformation of the motor (with a more fully closed cleft) in which we hypothesize that the HTH is only slightly repositioned while the HCM-loop can now dock on subdomain-3 of Actin-1. The creation of this higher-affinity state for F-actin is accompanied by the major lever arm swing and closure of the P_i channel (likely by a Switch-II conformational change) that prevents P_i rebinding for unloaded motors. It is not known if the major lever arm swing and cleft closure occur in one step (directly forming the Strong-ADP visualized by Cryo-EM studies) or if other ADP states (possibly differing in actin binding, switch-II position, or lever arm position) are populated during the powerstroke. The last step of the powerstroke leads to the Rigor state upon isomerization of the motor while strongly bound to F-actin. This isomerization is characterized by the untwisting of the transducer and the rotation of the N-term subdomain relative to the U50 subdomain (thus the actin interface). This leads to an additional lever arm reorientation (see Figure 11). ADP release is facilitated in this (ADP weakly bound/Rigor) state, since Mg^{2+} can no longer mediate interactions between the ^{U50}Switch-I and $^{N\text{-term}}$P-loop.[83] ATP binding in the Rigor state leads to the formation of the Post-Rigor state and actin detachment.[83,184] The recovery stroke allows the reformation of the state in which the lever arm is primed[86] and closure of the back door allows efficient ATP hydrolysis, trapping the motor in the Pre-powerstroke state. A

DOI: 10.1021/acs.chemrev.9b00264
Chem. Rev. XXXX, XXX, XXX−XXX

Figure 16. continued

new powerstroke is then initiated upon the association with F-actin. According to this model, the powerstroke is a multistep event representing transitions between several states once the motor is stereospecifically associated with the actin track. The experiments/concepts supporting this model (the chronology of the events and the features of the actin-bound states) are indicated in purple boxes.

the swing occurs at a rate that was greater than the rate at which P_i appears in solution. This initially led to the proposal that the lever arm swing must occur to allow the release of P_i,[177,178] rather than P_i leaving the active site must occur to allow cleft closure and swing of the lever arm.[61]

A number of studies have shown that increasing the P_i concentration in muscle fibers leads to a drop in force by decreasing the number of force-generating cross-bridges.[166,174,175,181−183] Experiments with step changes in $[P_i]$ (caged phosphate) were interpreted as demonstrating that P_i transient would be a two-step process requiring the reversal of the powerstroke; thus, the model proposed was that force production precedes the release of phosphate.[179] However, a later study calls into question this interpretation of the data.[174,176] Thus, this data is in agreement with the model we proposed:[60,61] the formation of the P_iR state is the initiation of the generation of force, which is then followed by P_i release and the powerstroke. In fact, both in muscle and in single molecule experiments,[167,168,180] phosphate only drops the force under conditions in which the lever arm swing is prevented. This implies that either P_i exit and entry into the myosin motor can only occur prior to the large component of the lever arm swing[60] or that strain can sufficiently alter the Strong-ADP bound heads to facilitate P_i re-entry in this state and reverse the powerstroke leading to detachment. However, the ATP consumption of cross-bridges under load at high concentrations of P_i argues against the second scenario.[181] The increase in Pi concentration favors re-entry of Pi in the early states of the powerstroke (PiR state) which leads to detachment of an ADP.Pi-bound head, consistent with low ATP consumption.

While studies have been interpreted as evidence for P_i release following the lever arm swing,[167,169,179,180] we noted above (see section 4.2) that recent optical trap experiments support[169] an open phosphate tunnel prior to the completion of the lever arm swing. A 1−3 pN load indeed increases the percentage of myosin heads that are detaching prior to the lever arm swing (so-called A_f and A_{int} in ref 169, which are presumably respectively in either a PPS or P_iR state of lower affinity than in the Strong-ADP state populated after a significant component of the lever arm swing). The 2-fold slower detachment of the myosin heads that have completed the lever arm swing (k_s) indicates that these heads cannot be directly sensitive to 10 mM P_i under these loaded conditions. What these experiments also indicate is that a 1−3 pN load is sufficient to greatly increase the detachment of heads in the early states of the powerstroke, i.e., in the P_iR state. This further supports that the actin binding interface in the early powerstroke states differs from and is weaker than that found in the Strong-ADP and Rigor states, although it is higher in actin affinity as compared to PPS.

Additional evidence that the state allowing release of P_i forms before the major component of the lever arm swing coupled to cleft closure came from the study of the cardiac myosin force-enhancing drug, omecamtiv mecarbil (OM). OM is able to stabilize both the Pre-powerstroke state and the P_iR state on actin.[21,22] It binds in a pocket that exists only in motors with a primed lever arm.[22] Binding of the drug thus results in blockage or slowing of the lever arm swing, as revealed by probes that sense lever arm movement,[185] as well as by measurements of lever arm swing in an optical trap.[186] However, OM accelerates P_i release from myosin, thus demonstrating that the P_iR state must form prior to lever arm swing (Figure 16).

What we have no insight into is what are the interactions that form between actin and myosin that lead to the rapid cleft closure. As with the formation of the P_iR state, this must be driven by interactions between actin and the myosin surface loops that can reposition themselves to contribute to a changing actin interface. It is likely that some actin−myosin interactions found in the P_iR state are maintained (especially hydrophobic interactions with the L50 subdomain, after possibly small local adaptations), while others may be lost (potentially those of the Activation-loop). We hypothesize that the exact interactions of the loops with actin change as the cleft closes and also will be different for different classes of myosin.

We do not know if the major swing of the lever arm coupled to cleft closure occurs in one continuous transition or is partitioned into multiple transitions that lever arm probes have not revealed. We do know that a probe near the C-terminus of actin (pyrene label on Cys374) senses some changes induced on the track by myosin upon the formation of the Strong MgADP binding state. What we do not know is what part of the final cleft closure occurs during this transition and how much of the lever arm swing is coupled to it. For many processive myosins (e.g., Myo5 and Myo6), the strong MgADP binding state is the predominant steady-state intermediate in the overall actin−myosin ATPase cycle.

The transition that follows the formation of the Strong MgADP state to release Mg^{2+} and ADP and create the rigor interface has been visualized by EM but not at sufficient resolution to discern differences that may occur in the actin interface and in the internal cleft. The affinity of the vast majority of myosins for actin in Rigor is higher than when MgADP is bound to myosin, although this difference is not as pronounced for some myosins. In fact, a notable exception is non-muscle myosin 2 isoforms for which the affinity for F-actin is greater when MgADP is bound. What we do not know is what rearrangements of the actin interface and surface loop positions must occur to allow this transition. Little is known also about how the internal sequences of the motor modulate this transition and how specific sequences (such as in N-terminal extensions[39,46,159] or the lever arm composition[39,46,68]) contribute to regulate this transition. Further investigations are required to reach a new understanding on force sensitivity and ability of motors to anchor and work under load.

The fact that release of MgADP requires a swing of the lever arm makes the rate of ADP release load-sensitive. In muscle, the slowing of ADP release results in a slowing of ATPase activity under load, which was recognized in 1923 and termed the Fenn effect.[187,188] More recently, it has been noted that myosins that have large lever arm swings associated with ADP release are particularly load-sensitive and can be adapted to

DOI: 10.1021/acs.chemrev.9b00264
Chem. Rev. XXXX, XXX, XXX−XXX

strain sensing as their primary role.[39,67,68,159,189] In addition, strain sensing is defined for myosins by their ability to reverse the transitions of the powerstroke from the Strong-ADP back to the P_iR state when they work under load[168]—a high-energy barrier for this transition defines good anchoring myosins.[67,68]

5. PERSPECTIVES: FUTURE STUDIES TO ADDRESS UNANSWERED QUESTIONS

The actin binding states that we described above have been detected by a combination of transient kinetic experiments and structural studies (both Cryo-EM and X-ray crystallography). Detection by kinetic experiments requires the existence of probes that do not alter the reactions but can sense transitions. This largely relies on detecting the release of the ATP hydrolysis products from myosin, as well as the one probe that senses changes in F-actin in response to some aspect of cleft closure in myosin (pyrene−actin quenching[141,148]). More recently, FRET probes have been introduced and allow the possibility of sensing additional transitions in the cycle. The position of the probes can be engineered into the myosins based on structural data related to the subdomains that are most likely to rearrange during transitions. Another important technical advance to augment the use of these probes is the development of high-time-resolution FRET,[177,178] which allows changes in FRET to be resolved at rates that can sense rapid transitions in the cycle. Indeed, such data are the basis of assigning a state that undergoes a rapid lever arm swing (likely coupled to cleft closure) immediately following formation of the P_iR state (Figure 16). This critical structural transition serves to drive the cycle forward unidirectionally (i.e., gating of the reaction) by ensuring that P_i will be released into solution and not re-enter the P_i tunnel (which must be disrupted during the transition).

Ultimately, though, a detailed structural understanding of the subdomain rearrangements and actin binding loop rearrangements during state transitions of the cycle on actin can only come from high-resolution structural studies. For EM, this will require ever-increasing resolution, coupled with strategies to trap the myosins in various states of the cycle. For X-ray studies, this will require small fragments of F-actin that can be cocrystallized with myosin trapped in distinct states of the cycle. It is likely that the general scheme of internal conformational changes within the motor domain throughout the cycle is relatively conserved among myosin classes. Whether essential elements in the actin binding loops are conserved to produce the powerstroke cannot be predicted. However, the variability of these loops suggests that they may give rise to different actin interactions for different myosin classes that both position the motor somewhat differently on actin as well as differentially tune the kinetic transitions.

All of the above discussions involve structures and kinetic transitions that take place in the absence of any load on the myosin. And yet we know first from studies with muscle fibers,[174,175,182,183] and with single myosin molecules of multiple classes,[67,168,186,190,191] that load has a profound effect on a subset of the kinetic transitions and that stretching of activated muscle causes detachment of cross-bridges that appears to be preceded by reversal of the powerstroke transitions.[192] Applying load to the force-generating myosin heads will manifest in distortions of compliant regions of the motor itself. EM reconstructions have allowed the direct visualization (at low resolution) of the strain imposed by one myosin head on the other in the case of a single two-headed Myo5 molecule walking on an actin track.[193,194] High-speed AFM studies also visualized changes in lever arm position but in real time.[195,196] In this case, the elements that are notably distorted by the strain are the lever arm and the position of the Converter, which likely are, with the transducer, a major source of compliance within the myosin motor itself. Kinetic studies on these same dimeric Myo5 molecules reveal that the compliance is sufficient to allow the lead head on actin to release P_i and close its internal cleft (but not release ADP), indicating that the major component of the lever arm swing occurs but cannot be completed.[197] This ensures that the lead head is strongly attached before the rear head detaches, thus optimizing processive movement on actin. Development of techniques to control load-dependent kinetics at the single-molecule level, such as harmonic force spectroscopy, provides a means to directly measure the effect of mutations or drug binding to myosin heads[198] in their load-sensitive steps. Studies of point mutations responsible for human diseases with structural and functional approaches will bring new insights into the force generation mechanism and its load dependence as well as much needed knowledge toward therapies for heart diseases. New strategies to further restrict lever arm movements may reveal additional complexities when coupled with higher-resolution Cryo-EM studies and perhaps someday even X-ray crystallography.

AUTHOR INFORMATION

Corresponding Author

*Phone: 33-(0)1-56-24-63-95. Fax: 33-(0)1-56-24-63-82. E-mail: anne.houdusse@curie.fr.

ORCID

Anne Houdusse: 0000-0002-8566-0336

Notes

The authors declare no competing financial interest.

Biographies

Julien Robert-Paganin, Ph.D., is a CNRS researcher in the *Structural Motility* team (since 2019). He received his Ph.D. from the Paris Descartes University in 2014, working on the RNA helicase Prp43 under the supervision of Dr. Stephane Réty. After six months of teaching in Physics (ATER position), he joined the *Structural Motility* team led by Dr. Anne Houdusse in 2015 as postdoctoral fellow. Dr. Paganin is a biophysicist and a crystallographer. His research focuses on the understanding of force production by myosin motors and how dysfunctions of these molecular motors lead to various diseases such as cardiomyopathies.

Olena Pylypenko, Ph.D., is a CNRS researcher in the Cell Biology and Cancer department (UMR144) at Curie Institute, Paris, France (since 2011). She received her Ph.D. from Heidelberg University in 2003 working on structural studies of cytochrome P450 proteins under supervision of Prof. Dr. Ilme Schlichting at the Max Planck Institute for Molecular Physiology, Dortmund, Germany. Then, she worked at the Physical Biochemistry department directed by Prof. Dr. Roger Goody as a postdoctoral fellow to study intracellular trafficking and Rab GTPases regulation. She joined the Structural Motility team led by Dr. Anne Houdusse at the Curie Institute, Paris, in 2007 to pursue research on molecular motors. A fellowship from the French Association for Cancer Research (ARC) foundation has supported this postdoctoral work for three years. Her current research interests include intracellular trafficking protein machineries, molecular motors, small GTPases, and their partners.

DOI: 10.1021/acs.chemrev.9b00264
Chem. Rev. XXXX, XXX, XXX−XXX

Carlos Kikuti, Ph.D., is a CNRS Research Associate (since 2011). He left Porecatu (Brazil) to study in the Universidade Federal de São Paulo (UNIFESP) where he obtained a M.Sc. degree in Kaethy Bisan Alves' laboratory in 2001 and his Ph.D. in Sergio Schenkman's laboratory in 2006. He moved to France for a postdoctoral position in Félix Rey's laboratory at the Pasteur Institute in 2006. He joined the Structural Motility team directed by Dr. Anne Houdusse (Curie Institute) in 2010 and has since been applying his expertise in Protein Structure, Biophysics, and Biochemistry to the study of a number of different molecular motors.

H. Lee Sweeney, Ph.D., is the director of the Myology Institute at University of Florida (UF), where he is also a professor of Pharmacology & Therapeutics. Prior to joining the faculty at UF, Dr. Sweeney was the William Maul Measey Professor and Chairman of Physiology at the University of Pennsylvania, where he is now an emeritus professor of Physiology. Dr. Sweeney received a bachelor's degree in Biochemistry from the Massachusetts Institute of Technology, a master's in Physiology from Harvard University, and a Ph.D. in Physiology and Biophysics from Harvard University. Dr. Sweeney's expertise spans cardiovascular disease, skeletal muscle disorders, and molecular motors of the myosin superfamily. He was elected as a fellow of the American Heart Association in 2001 and a fellow of the Biophysical Society in 2017 and has been the director of a Paul Wellstone Muscular Dystrophy Cooperative Center since 2005.

Anne Houdusse, Ph.D., is a CNRS research director in the Cell Biology and Cancer department (UMR144) at the Curie Institute, Paris, France. Dr. Houdusse was trained as a structural biologist and a chemist, earning a B.S. in chemistry from Ecole Normale Superieure and M.S. and Ph.D. degrees from the Pasteur Institute, Paris. Dr. Houdusse received a HFSPO fellowship in 1992 to study molecular motors at Brandeis University (Waltham, MA, USA) with Drs. Carolyn Cohen and Andrew Szent Györgyi. She received an ATIP award in 1999 and returned to Paris to establish her independent laboratory, the *Structural Motility* Team at the Curie Institute. The focus of her group's research has been on the understanding of how motors produce force and how they are recruited and regulated in cells. Dr. Houdusse received the CNRS Silver Medal and was elected as an EMBO member in 2013. Her contributions in the motor field have been recognized with a FEBS award for outstanding achievement in the field of Structural Biology in 2005, the FEBS/EMBO Women in Science Award in 2009, and the Prix Lecocq from the French Academy of Sciences in 2018.

ACKNOWLEDGMENTS

H.L.S. was supported by National Institutes of Health Grant DC009100. A.H. is supported by grants from CNRS, AFM 21805 and ANR-17-CE11-0029-01. The A.H. team is part of Labex CelTisPhyBio 11-LBX-0038 and IDEX PSL (ANR-10-IDEX-0001-02-PSL).

REFERENCES

(1) Titus, M. A. Myosin-Driven Intracellular Transport. Cold Spring Harb. *Cold Spring Harbor Perspect. Biol.* **2018**, *10*, a021972.
(2) Masters, T. A.; Kendrick-Jones, J.; Buss, F. Myosins: Domain Organisation, Motor Properties, Physiological Roles and Cellular Functions. *Handb. Exp. Pharmacol.* **2016**, *235*, 77−122.
(3) Heissler, S. M.; Sellers, J. R. Kinetic Adaptations of Myosins for Their Diverse Cellular Functions. *Traffic* **2016**, *17*, 839−859.
(4) Berg, J. S.; Powell, B. C.; Cheney, R. E. A Millennial Myosin Census. *Mol. Biol. Cell* **2001**, *12*, 780−794.
(5) Li, J.; Lu, Q.; Zhang, M. Structural Basis of Cargo Recognition by Unconventional Myosins in Cellular Trafficking. *Traffic* **2016**, *17*, 822−838.
(6) Heissler, S. M.; Sellers, J. R. Various Themes of Myosin Regulation. *J. Mol. Biol.* **2016**, *428*, 1927−1946.
(7) Sweeney, H. L.; Houdusse, A. Myosin VI Rewrites the Rules for Myosin Motors. *Cell* **2010**, *141*, 573−582.
(8) Zhang, N.; Yao, L.-L.; Li, X. Regulation of Class V Myosin. *Cell. Mol. Life Sci.* **2018**, *75*, 261−273.
(9) Wells, A. L.; Lin, A. W.; Chen, L.-Q.; Safer, D.; Cain, S. M.; Hasson, T.; Carragher, B. O.; Milligan, R. A.; Sweeney, H. L. Myosin VI Is an Actin-Based Motor That Moves Backwards. *Nature* **1999**, *401*, 505−508.
(10) Alamo, L.; Koubassova, N.; Pinto, A.; Gillilan, R.; Tsaturyan, A.; Padrón, R. Lessons from a Tarantula: New Insights into Muscle Thick Filament and Myosin Interacting-Heads Motif Structure and Function. *Biophys. Rev.* **2017**, *9*, 461−480.
(11) Alamo, L.; Pinto, A.; Sulbarán, G.; Mavárez, J.; Padrón, R. Lessons from a Tarantula: New Insights into Myosin Interacting-Heads Motif Evolution and Its Implications on Disease. *Biophys. Rev.* **2018**, *10*, 1465−1477.
(12) Trivedi, D. V.; Adhikari, A. S.; Sarkar, S. S.; Ruppel, K. M.; Spudich, J. A. Hypertrophic Cardiomyopathy and the Myosin Mesa: Viewing an Old Disease in a New Light. *Biophys. Rev.* **2018**, *10*, 27−48.
(13) Bloemink, M. J.; Geeves, M. A. Shaking the Myosin Family Tree: Biochemical Kinetics Defines Four Types of Myosin Motor. *Semin. Cell Dev. Biol.* **2011**, *22*, 961−967.
(14) De La Cruz, E. M.; Ostap, M. E. Relating Biochemistry and Function in the Myosin Superfamily. *Curr. Opin. Cell Biol.* **2004**, *16*, 61−67.
(15) Yotti, R.; Seidman, C. E.; Seidman, J. G. Advances in the Genetic Basis and Pathogenesis of Sarcomere Cardiomyopathies. *Annu. Rev. Genomics Hum. Genet.* **2019**, *20*, 129−153.
(16) Jungbluth, H.; Treves, S.; Zorzato, F.; Sarkozy, A.; Ochala, J.; Sewry, C.; Phadke, R.; Gautel, M.; Muntoni, F. Congenital Myopathies: Disorders of Excitation−Contraction Coupling and Muscle Contraction. *Nat. Rev. Neurol.* **2018**, *14*, 151−167.
(17) Spudich, J. A. Hypertrophic and Dilated Cardiomyopathy: Four Decades of Basic Research on Muscle Lead to Potential Therapeutic Approaches to These Devastating Genetic Diseases. *Biophys. J.* **2014**, *106*, 1236−1249.
(18) Robert-Paganin, J.; Auguin, D.; Houdusse, A. Hypertrophic Cardiomyopathy Disease Results from Disparate Impairments of Cardiac Myosin Function and Auto-Inhibition. *Nat. Commun.* **2018**, *9*, 4019.
(19) Avraham, K. B.; Hasson, T.; Steel, K. P.; Kingsley, D. M.; Russell, L. B.; Mooseker, M. S.; Copeland, N. G.; Jenkins, N. A. The Mouse Snell's Waltzer Deafness Gene Encodes an Unconventional Myosin Required for Structural Integrity of Inner Ear Hair Cells. *Nat. Genet.* **1995**, *11*, 369−375.
(20) Gotoh, N.; Yan, Q.; Du, Z.; Biemesderfer, D.; Kashgarian, M.; Mooseker, M. S.; Wang, T. Altered Renal Proximal Tubular Endocytosis and Histology in Mice Lacking Myosin-VI. *Cytoskeleton* **2010**, *67*, 178−192.
(21) Malik, F. I.; Hartman, J. J.; Elias, K. A.; Morgan, B. P.; Rodriguez, H.; Brejc, K.; Anderson, R. L.; Sueoka, S. H.; Lee, K. H.; Finer, J. T.; et al. Cardiac Myosin Activation: A Potential Therapeutic Approach for Systolic Heart Failure. *Science* **2011**, *331*, 1439−1443.
(22) Planelles-Herrero, V. J.; Hartman, J. J.; Robert-Paganin, J.; Malik, F. I.; Houdusse, A. Mechanistic and Structural Basis for Activation of Cardiac Myosin Force Production by Omecamtiv Mecarbil. *Nat. Commun.* **2017**, *8*, 190.
(23) Green, E. M.; Wakimoto, H.; Anderson, R. L.; Evanchik, M. J.; Gorham, J. M.; Harrison, B. C.; Henze, M.; Kawas, R.; Oslob, J. D.; Rodriguez, H. M.; et al. A Small-Molecule Inhibitor of Sarcomere Contractility Suppresses Hypertrophic Cardiomyopathy in Mice. *Science* **2016**, *351*, 617−621.
(24) Kawas, R. F.; Anderson, R. L.; Ingle, S. R. B.; Song, Y.; Sran, A. S.; Rodriguez, H. M. A Small-Molecule Modulator of Cardiac Myosin Acts on Multiple Stages of the Myosin Chemomechanical Cycle. *J. Biol. Chem.* **2017**, *292*, 16571−16577.

DOI: 10.1021/acs.chemrev.9b00264
Chem. Rev. XXXX, XXX, XXX−XXX

(25) Rohde, J. A.; Roopnarine, O.; Thomas, D. D.; Muretta, J. M. Mavacamten Stabilizes an Autoinhibited State of Two-Headed Cardiac Myosin. *Proc. Natl. Acad. Sci. U. S. A.* **2018**, *115*, E7486−E7494.
(26) Anderson, R. L.; Trivedi, D. V.; Sarkar, S. S.; Henze, M.; Ma, W.; Gong, H.; Rogers, C. S.; Gorham, J. M.; Wong, F. L.; Morck, M. M.; et al. Deciphering the Super Relaxed State of Human β-Cardiac Myosin and the Mode of Action of Mavacamten from Myosin Molecules to Muscle Fibers. *Proc. Natl. Acad. Sci. U. S. A.* **2018**, *115*, E8143−E8152.
(27) Liu, Y.; White, H. D.; Belknap, B.; Winkelmann, D. A.; Forgacs, E. Omecamtiv Mecarbil Modulates the Kinetic and Motile Properties of Porcine β-Cardiac Myosin. *Biochemistry* **2015**, *54*, 1963−1975.
(28) Ydenberg, C. A.; Smith, B. A.; Breitsprecher, D.; Gelles, J.; Goode, B. L. Cease-fire at the Leading Edge: New Perspectives on Actin Filament Branching, Debranching, and Cross-linking. *Cytoskeleton* **2011**, *68*, 596−602.
(29) Blanchoin, L.; Boujemaa-Paterski, R.; Sykes, C.; Plastino, J. Actin Dynamics, Architecture, and Mechanics in Cell Motility. *Physiol. Rev.* **2014**, *94*, 235−263.
(30) Kabsch, W.; Mannherz, H.; Suck, D.; Pai, E. F.; Holmes, K. C. Atomic Structure of the Actin: DNase I Complex. *Nature* **1990**, *347*, 37−44.
(31) Oda, T.; Iwasa, M.; Aihara, T.; Maéda, Y.; Narita, A. The Nature of the Globular- to Fibrous-Actin Transition. *Nature* **2009**, *457*, 441−445.
(32) Chou, S. Z.; Pollard, T. D. Mechanism of Actin Polymerization Revealed by Cryo-EM Structures of Actin Filaments with Three Different Bound Nucleotides. *Proc. Natl. Acad. Sci. U. S. A.* **2019**, *116*, 4265−4274.
(33) Merino, F.; Pospich, S.; Funk, J.; Wagner, T.; Küllmer, F.; Arndt, H.-D.; Bieling, P.; Raunser, S. Structural Transitions of F-Actin upon ATP Hydrolysis at near-Atomic Resolution Revealed by Cryo-EM. *Nat. Struct. Mol. Biol.* **2018**, *25*, 528−537.
(34) Otterbein, L. R.; Graceffa, P.; Dominguez, R. The Crystal Structure of Uncomplexed Actin in the ADP State. *Science* **2001**, *293*, 708−711.
(35) Holmes, K. C.; Popp, D.; Gebhard, W.; Kabsch, W. Atomic Model of the Actin Filament. *Nature* **1990**, *347*, 44−49.
(36) von der Ecken, J.; Heissler, S. M.; Pathan-Chhatbar, S.; Manstein, D. J.; Raunser, S. Cryo-EM Structure of a Human Cytoplasmic Actomyosin Complex at near-Atomic Resolution. *Nature* **2016**, *534*, 724−728.
(37) Oda, T.; Namba, K.; Maéda, Y. Position and Orientation of Phalloidin in F-Actin Determined by X-Ray Fiber Diffraction Analysis. *Biophys. J.* **2005**, *88*, 2727−2736.
(38) Pospich, S.; Kumpula, E.-P.; von der Ecken, J.; Vahokoski, J.; Kursula, I.; Raunser, S. Near-Atomic Structure of Jasplakinolide-Stabilized Malaria Parasite F-Actin Reveals the Structural Basis of Filament Instability. *Proc. Natl. Acad. Sci. U. S. A.* **2017**, *114*, 10636−10641.
(39) Mentes, A.; Huehn, A.; Liu, X.; Zwolak, A.; Dominguez, R.; Shuman, H.; Ostap, M. E.; Sindelar, C. V. High-Resolution Cryo-EM Structures of Actin-Bound Myosin States Reveal the Mechanism of Myosin Force Sensing. *Proc. Natl. Acad. Sci. U. S. A.* **2018**, *115*, 1292−1297.
(40) McGough, A.; Pope, B.; Chiu, W.; Weeds, A. Cofilin Changes the Twist of F-Actin: Implications for Actin Filament Dynamics and Cellular Function. *J. Cell Biol.* **1997**, *138*, 771−781.
(41) Galkin, V. E.; Orlova, A.; Lukoyanova, N.; Wriggers, W.; Egelman, E. H. Actin Depolymerizing Factor Stabilizes an Existing State of F-Actin and Can Change the Tilt of F-Actin Subunits. *J. Cell Biol.* **2001**, *153*, 75−86.
(42) Huehn, A.; Cao, W.; Elam, A. W.; Liu, X.; Cruz, E.; Sindelar, C. V. The Actin Filament Twist Changes Abruptly at Boundaries between Bare and Cofilin-Decorated Segments. *J. Biol. Chem.* **2018**, *293*, 5377−5383.
(43) Tanaka, K.; Takeda, S.; Mitsuoka, K.; Oda, T.; Kimura-Sakiyama, C.; Maéda, Y.; Narita, A. Structural Basis for Cofilin Binding and Actin Filament Disassembly. *Nat. Commun.* **2018**, *9*, 1860.
(44) Blanchoin, L.; Pollard, T. D. Mechanism of Interaction of Acanthamoeba Actophorin (ADF/Cofilin) with Actin Filaments. *J. Biol. Chem.* **1999**, *274*, 15538−15546.
(45) Boussouf, S. E.; Geeves, M. A. Tropomyosin and Troponin Cooperativity on the Thin Filament. *Adv. Exp. Med. Biol.* **2007**, *592*, 99−109.
(46) Robert-Paganin, J.; Robblee, J. P.; Auguin, D.; Blake, T. C.; Bookwalter, C. S.; Krementsova, E. B.; Moussaoui, D.; Previs, M. J.; Jousset, G.; Baum, J.; et al. Plasmodium Myosin A Drives Parasite Invasion by an Atypical Force Generating Mechanism. *Nat. Commun.* **2019**, *10*, 3286.
(47) Heissler, S. M.; Sellers, J. R. Myosin Light Chains: Teaching Old Dogs New Tricks. *Bioarchitecture* **2014**, *4*, 169−188.
(48) Knight, P. J.; Thirumurugan, K.; Xu, Y.; Wang, F.; Kalverda, A. P.; Stafford, W. F.; Sellers, J. R.; Peckham, M. The Predicted Coiled-Coil Domain of Myosin 10 Forms a Novel Elongated Domain That Lengthens the Head. *J. Biol. Chem.* **2005**, *280*, 34702−34708.
(49) Batchelor, M.; Wolny, M.; Dougan, L.; Paci, E.; Knight, P. J.; Peckham, M. Myosin Tails and Single α-Helical Domains. *Biochem. Soc. Trans.* **2015**, *43*, 58−63.
(50) Hokanson, D. E.; Laakso, J. M.; Lin, T.; Sept, D.; Ostap, M. E. Myo1c Binds Phosphoinositides through a Putative Pleckstrin Homology Domain. *Mol. Biol. Cell* **2006**, *17*, 4856−4865.
(51) Spudich, G.; Chibalina, M. V.; Au, J.; Arden, S. D.; Buss, F.; Kendrick-Jones, J. Myosin VI Targeting to Clathrin-Coated Structures and Dimerization Is Mediated by Binding to Disabled-2 and PtdIns(4,5)P2. *Nat. Cell Biol.* **2007**, *9*, 176−183.
(52) Umeki, N.; Jung, H.; Sakai, T.; Sato, O.; Ikebe, R.; Ikebe, M. Phospholipid-Dependent Regulation of the Motor Activity of Myosin X. *Nat. Struct. Mol. Biol.* **2011**, *18*, 783−788.
(53) Rayment, I.; Rypniewski, W.; Schmidt-Base, K.; Smith, R.; Tomchick, D.; Benning, M.; Winkelmann, D.; Wesenberg, G.; Holden, H. Three-Dimensional Structure of Myosin Subfragment-1: A Molecular Motor. *Science* **1993**, *261*, 50−58.
(54) Fisher, A.; Smith, C.; Thoden, J.; Smith, R.; Sutoh, K.; Holden, H.; Rayment, I. X-Ray Structures of the Myosin Motor Domain of Dictyostelium Discoideum Complexed with MgADP.BeFx and MgADP.AlF4. *Biochemistry* **1995**, *34*, 8960−8972.
(55) Dominguez, R.; Freyzon, Y.; Trybus, K. M.; Cohen, C. Crystal Structure of a Vertebrate Smooth Muscle Myosin Motor Domain and Its Complex with the Essential Light Chain Visualization of the Pre−Power Stroke State. *Cell* **1998**, *94*, 559−571.
(56) Houdusse, A.; Kalabokis, V. N.; Himmel, D.; Szent-Györgyi, A. G.; Cohen, C. Atomic Structure of Scallop Myosin Subfragment S1 Complexed with MgADP: A Novel Conformation of the Myosin Head. *Cell* **1999**, *97*, 459−470.
(57) Houdusse, A.; Szent-Györgyi, A.; Cohen, C. Three Conformational States of Scallop Myosin S1. *Proc. Natl. Acad. Sci. U. S. A.* **2000**, *97*, 11238−11243.
(58) Coureux, P.-D.; Wells, A. L.; Ménétrey, J.; Yengo, C. M.; Morris, C. A.; Sweeney, H. L.; Houdusse, A. A Structural State of the Myosin V Motor without Bound Nucleotide. *Nature* **2003**, *425*, 419−423.
(59) Holmes, K. C.; Angert, I.; Kull, J. F.; Jahn, W.; Schröder, R. R. Electron Cryo-Microscopy Shows How Strong Binding of Myosin to Actin Releases Nucleotide. *Nature* **2003**, *425*, 423−427.
(60) Llinas, P.; Isabet, T.; Song, L.; Ropars, V.; Zong, B.; Benisty, H.; Sirigu, S.; Morris, C.; Kikuti, C.; Safer, D.; et al. How Actin Initiates the Motor Activity of Myosin. *Dev. Cell* **2015**, *33*, 401−412.
(61) Houdusse, A.; Sweeney, H. L. How Myosin Generates Force on Actin Filaments. *Trends Biochem. Sci.* **2016**, *41*, 989−997.
(62) Sweeney, H. L.; Houdusse, A. Structural and Functional Insights into the Myosin Motor Mechanism. *Annu. Rev. Biophys.* **2010**, *39*, 539−557.
(63) Gourinath, S.; Himmel, D. M.; Brown, J. H.; Reshetnikova, L.; Szent-Györgyi, A. G.; Cohen, C. Crystal Structure of Scallop Myosin

DOI: 10.1021/acs.chemrev.9b00264
Chem. Rev. XXXX, XXX, XXX−XXX

S1 in the Pre-Power Stroke State to 2.6 Å Resolution: Flexibility and Function in the Head. *Structure* **2003**, *11*, 1621−1627.
(64) Wang, F.; Kovács, M.; Hu, A.; Limouze, J.; Harvey, E. V.; Sellers, J. R. Kinetic Mechanism of Non-Muscle Myosin IIB Functional Adaptations for Tension Generation and Maintenance. *J. Biol. Chem.* **2003**, *278*, 27439−27448.
(65) Kovács, M.; Wang, F.; Hu, A.; Zhang, Y.; Sellers, J. R. Functional Divergence of Human Cytoplasmic Myosin II Kinetic Characterization of the Non-Muscle IIA Isoform. *J. Biol. Chem.* **2003**, *278*, 38132−38140.
(66) Chinthalapudi, K.; Heissler, S. M.; Preller, M.; Sellers, J. R.; Manstein, D. J. Mechanistic Insights into the Active Site and Allosteric Communication Pathways in Human Nonmuscle Myosin-2C. *eLife* **2017**, *6*, No. e32742.
(67) Laakso, J. M.; Lewis, J. H.; Shuman, H.; Ostap, M. E. Myosin I Can Act As a Molecular Force Sensor. *Science* **2008**, *321*, 133−136.
(68) Laakso, J. M.; Lewis, J. H.; Shuman, H.; Ostap, M. E. Control of Myosin-I Force Sensing by Alternative Splicing. *Proc. Natl. Acad. Sci. U. S. A.* **2010**, *107*, 698−702.
(69) Huxley, A. F. 6 Muscle Structure and Theories of Contraction. *Prog. Biophys. Biophys. Chem.* **1957**, *7*, 255−318.
(70) Huxley, A.; Simmons, R. Proposed Mechanism of Force Generation in Striated Muscle. *Nature* **1971**, *233*, 533−538.
(71) Lymn, R. W.; Taylor, E. W. Transient State Phosphate Production in the Hydrolysis of Nucleoside Triphosphates by Myosin. *Biochemistry* **1970**, *9*, 2975−2983.
(72) Biosca, J.; Travers, F.; Barman, T.; Bertrand, R.; Audemard, E.; Kassab, R. Transient Kinetics of ATP Hydrolysis by Covalently Crosslinked Actomyosin Complex in Water and 40% Ethylene Glycol by the Rapid Flow Quench Method. *Biochemistry* **1985**, *24*, 3814−3820.
(73) Bagshaw, C.; Trentham, D. The Reversibility of Adenosine Triphosphate Cleavage by Myosin. *Biochem. J.* **1973**, *133*, 323−328.
(74) Mannherz, H.; Schenck, H.; Goody, R. S. Synthesis of ATP from ADP and Inorganic Phosphate at the Myosin-Subfragment 1 Active Site. *Eur. J. Biochem.* **1974**, *48*, 287−295.
(75) Huxley, H. The Mechanism of Muscular Contraction. *Science* **1969**, *164*, 1356−1366.
(76) Huxley, H.; Reconditi, M.; Stewart, A.; Irving, T. X-Ray Interference Studies of Crossbridge Action in Muscle Contraction: Evidence from Quick Releases. *J. Mol. Biol.* **2006**, *363*, 743−761.
(77) Geeves, M.; Holmes, K. Structural Mechanism of Muscle Contraction. *Annu. Rev. Biochem.* **1999**, *68*, 687−728.
(78) Whittaker, M.; Wilson-Kubalek, E. M.; Smith, J. E.; Faust, L.; Milligan, R. A.; Sweeney, H. L. A 35-Å Movement of Smooth Muscle Myosin on ADP Release. *Nature* **1995**, *378*, 748−751.
(79) Uyeda, T.; Abramson, P.; Spudich, J. The Neck Region of the Myosin Motor Domain Acts as a Lever Arm to Generate Movement. *Proc. Natl. Acad. Sci. U. S. A.* **1996**, *93*, 4459−4464.
(80) Tyska, M. J.; Warshaw, D. M. The Myosin Power Stroke. *Cell Motil. Cytoskeleton* **2002**, *51*, 1−15.
(81) Veigel, C.; Coluccio, L. M.; Jontes, J. D.; Sparrow, J. C.; Milligan, R. A.; Molloy, J. E. The Motor Protein Myosin-I Produces Its Working Stroke in Two Steps. *Nature* **1999**, *398*, 530−533.
(82) Houdusse, A.; Cohen, C. Structure of the Regulatory Domain of Scallop Myosin at 2 Å Resolution: Implications for Regulation. *Structure* **1996**, *4*, 21−32.
(83) Coureux, P.; Sweeney, H. L.; Houdusse, A. Three Myosin V Structures Delineate Essential Features of Chemo-mechanical Transduction. *EMBO J.* **2004**, *23*, 4527−4537.
(84) Yang, Y.; Gourinath, S.; Kovács, M.; Nyitray, L.; Reutzel, R.; Himmel, D. M.; O'Neall-Hennessey, E.; Reshetnikova, L.; Szent-Györgyi, A. G.; Brown, J. H.; et al. Rigor-like Structures from Muscle Myosins Reveal Key Mechanical Elements in the Transduction Pathways of This Allosteric Motor. *Structure* **2007**, *15*, 553−564.
(85) Risal, D.; Gourinath, S.; Himmel, D. M.; Szent-Györgyi, A. G.; Cohen, C. Myosin Subfragment 1 Structures Reveal a Partially Bound Nucleotide and a Complex Salt Bridge That Helps Couple Nucleotide and Actin Binding. *Proc. Natl. Acad. Sci. U. S. A.* **2004**, *101*, 8930−8935.
(86) Blanc, F.; Isabet, T.; Benisty, H.; Sweeney, H. L.; Cecchini, M.; Houdusse, A. An Intermediate along the Recovery Stroke of Myosin VI Revealed by X-Ray Crystallography and Molecular Dynamics. *Proc. Natl. Acad. Sci. U. S. A.* **2018**, *115*, 6213−6218.
(87) Smith, C.; Rayment, I. X-Ray Structure of the Magnesium-(II).ADP.Vanadate Complex of the Dictyostelium Discoideum Myosin Motor Domain to 1.9 A Resolution. *Biochemistry* **1996**, *35*, 5404−5417.
(88) Yengo, C. M.; Cruz, E.; Safer, D.; Ostap, M. E.; Sweeney, H. L. Kinetic Characterization of the Weak Binding States of Myosin V. *Biochemistry* **2002**, *41*, 8508−8517.
(89) Nagy, A.; Takagi, Y.; Billington, N.; Sun, S. A.; Hong, D. K.; Homsher, E.; Wang, A.; Sellers, J. R. Kinetic Characterization of Nonmuscle Myosin IIB at the Single Molecule Level. *J. Biol. Chem.* **2013**, *288*, 709−722.
(90) Yount, R.; Lawson, D.; Rayment, I. Is Myosin a "Back Door" Enzyme?. *Biophys. J.* **1995**, *68*, 44S−47S; discussion 47S−49S.
(91) Woodward, S.; Eccleston, J.; Geeves, M. Kinetics of the Interaction of 2'(3')-O-(N-Methylanthraniloyl)-ATP with Myosin Subfragment 1 and Actomyosin Subfragment 1: Characterization of Two Acto-S1-ADP Complexes. *Biochemistry* **1991**, *30*, 422−430.
(92) Geeves, M.; Conibear, P. The Role of Three-State Docking of Myosin S1 with Actin in Force Generation. *Biophys. J.* **1995**, *68*, 194S−199S; discussion 199S−201S.
(93) Jontes, J. D.; Wilson-Kubalek, E. M.; Milligan, R. A. A 32° Tail Swing in Brush Border Myosin I on ADP Release. *Nature* **1995**, *378*, 751−753.
(94) Wulf, S. F.; Ropars, V.; Fujita-Becker, S.; Oster, M.; Hofhaus, G.; Trabuco, L. G.; Pylypenko, O.; Sweeney, H. L.; Houdusse, A. M.; Schröder, R. R. Force-Producing ADP State of Myosin Bound to Actin. *Proc. Natl. Acad. Sci. U. S. A.* **2016**, *113*, E1844−E1852.
(95) Gurel, P. S.; Kim, L. Y.; Ruijgrok, P. V.; Omabegho, T.; Bryant, Z.; Alushin, G. M. Cryo-EM Structures Reveal Specialization at the Myosin VI-Actin Interface and a Mechanism of Force Sensitivity. *eLife* **2017**, *6*, No. e31125.
(96) Sakamoto, T.; Yildiz, A.; Selvin, P. R.; Sellers, J. R. Step-Size Is Determined by Neck Length in Myosin V. *Biochemistry* **2005**, *44*, 16203−16210.
(97) Purcell, T. J.; Morris, C.; Spudich, J. A.; Sweeney, H. L. Role of the Lever Arm in the Processive Stepping of Myosin V. *Proc. Natl. Acad. Sci. U. S. A.* **2002**, *99*, 14159−14164.
(98) Moore, J. R.; Krementsova, E. B.; Trybus, K. M.; Warshaw, D. M. Does the Myosin V Neck Region Act as a Lever? *J. Muscle Res. Cell Motil.* **2004**, *25*, 29−35.
(99) Ropars, V.; Yang, Z.; Isabet, T.; Blanc, F.; Zhou, K.; Lin, T.; Liu, X.; Hissier, P.; Samazan, F.; Amigues, B.; et al. The Myosin X Motor Is Optimized for Movement on Actin Bundles. *Nat. Commun.* **2016**, *7*, 12456.
(100) Sato, O.; Jung, H.; Komatsu, S.; Tsukasaki, Y.; Watanabe, T. M.; Homma, K.; Ikebe, M. Activated Full-Length Myosin-X Moves Processively on Filopodia with Large Steps toward Diverse Two-Dimensional Directions. *Sci. Rep.* **2017**, *7*, 44237.
(101) Lu, Q.; Ye, F.; Wei, Z.; Wen, Z.; Zhang, M. Antiparallel Coiled-Coil−Mediated Dimerization of Myosin X. *Proc. Natl. Acad. Sci. U. S. A.* **2012**, *109*, 17388−17393.
(102) Vavra, K. C.; Xia, Y.; Rock, R. S. Competition between Coiled-Coil Structures and the Impact on Myosin-10 Bundle Selection. *Biophys. J.* **2016**, *110*, 2517−2527.
(103) Iwaki, M.; Iwane, A. H.; Shimokawa, T.; Cooke, R.; Yanagida, T. Brownian Search-and-Catch Mechanism for Myosin-VI Steps. *Nat. Chem. Biol.* **2009**, *5*, 403−405.
(104) Karagiannis, P.; Ishii, Y.; Yanagida, T. Molecular Machines Like Myosin Use Randomness to Behave Predictably. *Chem. Rev.* **2014**, *114*, 3318−3334.
(105) Gebhardt, C. J.; Clemen, A.; Jaud, J.; Rief, M. Myosin-V Is a Mechanical Ratchet. *Proc. Natl. Acad. Sci. U. S. A.* **2006**, *103*, 8680−8685.

DOI: 10.1021/acs.chemrev.9b00264
Chem. Rev. XXXX, XXX, XXX−XXX

(106) Müller, M.; Diensthuber, R. P.; Chizhov, I.; Claus, P.; Heissler, S. M.; Preller, M.; Taft, M. H.; Manstein, D. J. Distinct Functional Interactions between Actin Isoforms and Nonsarcomeric Myosins. *PLoS One* **2013**, *8*, No. e70636.
(107) Barua, B.; Nagy, A.; Sellers, J. R.; Hitchcock-DeGregori, S. E. Regulation of Nonmuscle Myosin II by Tropomyosin. *Biochemistry* **2014**, *53*, 4015−4024.
(108) Manstein, D. J.; Mulvihill, D. P. Tropomyosin-Mediated Regulation of Cytoplasmic Myosins. *Traffic* **2016**, *17*, 872−877.
(109) Gateva, G.; Kremneva, E.; Reindl, T.; Kotila, T.; Kogan, K.; Gressin, L.; Gunning, P. W.; Manstein, D. J.; Michelot, A.; Lappalainen, P. Tropomyosin Isoforms Specify Functionally Distinct Actin Filament Populations In Vitro. *Curr. Biol.* **2017**, *27*, 705−713.
(110) Ménétrey, J.; Bahloul, A.; Wells, A. L.; Yengo, C. M.; Morris, C. A.; Sweeney, H. L.; Houdusse, A. The Structure of the Myosin VI Motor Reveals the Mechanism of Directionality Reversal. *Nature* **2005**, *435*, 779−785.
(111) Ménétrey, J.; Llinas, P.; Mukherjea, M.; Sweeney, H. L.; Houdusse, A. The Structural Basis for the Large Powerstroke of Myosin VI. *Cell* **2007**, *131*, 300−308.
(112) Spudich, J. A. Three Perspectives on the Molecular Basis of Hypercontractility Caused by Hypertrophic Cardiomyopathy Mutations. *Pfluegers Arch.* **2019**, *471*, 701−717.
(113) Pylypenko, O.; Song, L.; Shima, A.; Yang, Z.; Houdusse, A. M.; Sweeney, H. L. Myosin VI Deafness Mutation Prevents the Initiation of Processive Runs on Actin. *Proc. Natl. Acad. Sci. U. S. A.* **2015**, *112*, E1201−E1209.
(114) Kronert, W. A.; Melkani, G. C.; Melkani, A.; Bernstein, S. I. Alternative Relay and Converter Domains Tune Native Muscle Myosin Isoform Function in Drosophila. *J. Mol. Biol.* **2012**, *416*, 543−557.
(115) Miller, B. M.; Bloemink, M. J.; Nyitrai, M.; Bernstein, S. I.; Geeves, M. A. A Variable Domain near the ATP-Binding Site in Drosophila Muscle Myosin Is Part of the Communication Pathway between the Nucleotide and Actin-Binding Sites. *J. Mol. Biol.* **2007**, *368*, 1051−1066.
(116) Yang, C.; Ramanath, S.; Kronert, W. A.; Bernstein, S. I.; Maughan, D. W.; Swank, D. M. Alternative Versions of the Myosin Relay Domain Differentially Respond to Load to Influence Drosophila Muscle Kinetics. *Biophys. J.* **2008**, *95*, 5228−5237.
(117) Fujii, T.; Iwane, A. H.; Yanagida, T.; Namba, K. Direct Visualization of Secondary Structures of F-Actin by Electron Cryomicroscopy. *Nature* **2010**, *467*, 724−728.
(118) Murakami, K.; Yasunaga, T.; Noguchi, T.; Gomibuchi, Y.; Ngo, K. X.; Uyeda, T.; Wakabayashi, T. Structural Basis for Actin Assembly, Activation of ATP Hydrolysis, and Delayed Phosphate Release. *Cell* **2010**, *143*, 275−287.
(119) Rayment, I.; Holden, H.; Whittaker, M.; Yohn, C.; Lorenz, M.; Holmes, K.; Milligan, R. Structure of the Actin-Myosin Complex and Its Implications for Muscle Contraction. *Science* **1993**, *261*, 58−65.
(120) Schröder, R. R.; Manstein, D. J.; Jahn, W.; Holden, H.; Rayment, I.; Holmes, K. C.; Spudich, J. A. Three-Dimensional Atomic Model of F-Actin Decorated with Dictyostelium Myosin S1. *Nature* **1993**, *364*, 171−174.
(121) Behrmann, E.; Müller, M.; Penczek, P. A.; Mannherz, H.; Manstein, D. J.; Raunser, S. Structure of the Rigor Actin-Tropomyosin-Myosin Complex. *Cell* **2012**, *150*, 327−338.
(122) Volkmann, N.; Hanein, D.; Ouyang, G.; Trybus, K. M.; DeRosier, D. J.; Lowey, S. Evidence for Cleft Closure in Actomyosin upon ADP Release. *Nat. Struct. Biol.* **2000**, *7*, 1147−1155.
(123) De La Cruz, E. M.; Wells, A. L.; Rosenfeld, S. S.; Ostap, E. M.; Sweeney, H. L. The Kinetic Mechanism of Myosin V. *Proc. Natl. Acad. Sci. U. S. A.* **1999**, *96*, 13726−13731.
(124) Reubold, T. F.; Eschenburg, S.; Becker, A.; Kull, J. F.; Manstein, D. J. A Structural Model for Actin-Induced Nucleotide Release in Myosin. *Nat. Struct. Mol. Biol.* **2003**, *10*, 826−830.
(125) Geeves, M. A.; Holmes, K. C. Advances in Protein Chemistry. *Adv. Protein Chem.* **2005**, *71*, 161−193.
(126) Rosenfeld, S. S.; Houdusse, A.; Sweeney, H. L. Magnesium Regulates ADP Dissociation from Myosin V. *J. Biol. Chem.* **2005**, *280*, 6072−6079.
(127) Fujita-Becker, S.; Dürrwang, U.; Erent, M.; Clark, R. J.; Geeves, M. A.; Manstein, D. J. Changes in Mg2+ Ion Concentration and Heavy Chain Phosphorylation Regulate the Motor Activity of a Class I Myosin. *J. Biol. Chem.* **2005**, *280*, 6064−6071.
(128) Sidhu, N.; Dawson, J. F. A Crosslinked and Ribosylated Actin Trimer Does Not Interact Productively with Myosin. *Biochem. Cell Biol.* **2019**, *97*, 140−147.
(129) Takeda, S.; Narita, A.; Oda, T.; Tanaka, K.; Koike, R.; Ota, M.; Fujiwara, I.; Watanabe, N.; Maeda, Y. F-Form Actin Crystal Structures: Mechanisms of Actin Assembly and F-Actin ATP-Hydrolysis. *Biophys. J.* **2018**, *114*, 381a.
(130) Qu, Z.; Fujita-Becker, S.; Ballweber, E.; Ince, S.; Herrmann, C.; Schröder, R. R.; Mannherz, H. Interaction of Isolated Cross-linked Short Actin Oligomers with the Skeletal Muscle Myosin Motor Domain. *FEBS J.* **2018**, *285*, 1715−1729.
(131) Pospich, S.; Raunser, S. Single Particle Cryo-EM—an Optimal Tool to Study Cytoskeletal Proteins. *Curr. Opin. Struct. Biol.* **2018**, *52*, 16−24.
(132) Kucukelbir, A.; Sigworth, F. J.; Tagare, H. D. Quantifying the Local Resolution of Cryo-EM Density Maps. *Nat. Methods* **2014**, *11*, 63−65.
(133) Rosenthal, P. B.; Henderson, R. Optimal Determination of Particle Orientation, Absolute Hand, and Contrast Loss in Single-Particle Electron Cryomicroscopy. *J. Mol. Biol.* **2003**, *333*, 721−745.
(134) Milligan, R. Protein-Protein Interactions in the Rigor Actomyosin Complex. *Proc. Natl. Acad. Sci. U. S. A.* **1996**, *93*, 21−26.
(135) Banerjee, C.; Hu, Z.; Huang, Z.; Warrington, A. J.; Taylor, D. W.; Trybus, K. M.; Lowey, S.; Taylor, K. A. The Structure of the Actin-Smooth Muscle Myosin Motor Domain Complex in the Rigor State. *J. Struct. Biol.* **2017**, *200*, 325−333.
(136) Fujii, T.; Namba, K. Structure of Actomyosin Rigour Complex at 5.2 Å Resolution and Insights into the ATPase Cycle Mechanism. *Nat. Commun.* **2017**, *8*, 13969.
(137) Cope, J. M.; Whisstock, J.; Rayment, I.; Kendrick-Jones, J. Conservation within the Myosin Motor Domain: Implications for Structure and Function. *Structure* **1996**, *4*, 969−987.
(138) Bement, W. M.; Mooseker, M. S. TEDS Rule: A Molecular Rationale for Differential Regulation of Myosins by Phosphorylation of the Heavy Chain Head. *Cell Motil. Cytoskeleton* **1995**, *31*, 87−92.
(139) Clark, R.; Ansari, M.; Dash, S.; Geeves, M. A.; Coluccio, L. M. Loop 1 of Transducer Region in Mammalian Class I Myosin, Myo1b, Modulates Actin Affinity, ATPase Activity, and Nucleotide Access. *J. Biol. Chem.* **2005**, *280*, 30935−30942.
(140) Olivares, A. O.; Chang, W.; Mooseker, M. S.; Hackney, D. D.; Cruz, E. M. The Tail Domain of Myosin Va Modulates Actin Binding to One Head. *J. Biol. Chem.* **2006**, *281*, 31326−31336.
(141) De La Cruz, E. M.; Ostap, E. M.; Sweeney, H. L. Kinetic Mechanism and Regulation of Myosin VI. *J. Biol. Chem.* **2001**, *276*, 32373−32381.
(142) Valentin-Ranc, C.; Combeau, C.; Carlier, M.; Pantaloni, D. Myosin Subfragment-1 Interacts with Two G-Actin Molecules in the Absence of ATP. *J. Biol. Chem.* **1991**, *266*, 17872−17879.
(143) Woodrum, D.; Rich, S.; Pollard, T. Evidence for Biased Bidirectional Polymerization of Actin Filaments Using Heavy Meromyosin Prepared by an Improved Method. *J. Cell Biol.* **1975**, *67*, 231−237.
(144) Orlova, A.; Egelman, E. H. Cooperative Rigor Binding of Myosin to Actin Is a Function of F-Actin Structure. *J. Mol. Biol.* **1997**, *265*, 469−474.
(145) Thomas, D. D.; Prochniewicz, E.; Roopnarine, O. Changes in Actin and Myosin Structural Dynamics Due to Their Weak and Strong Interactions. *Results Probl. Cell Differ.* **2002**, *36*, 7−19.
(146) Galkin, V. E.; Orlova, A.; Egelman, E. H. Actin Filaments as Tension Sensors. *Curr. Biol.* **2012**, *22*, R96−R101.

DOI: 10.1021/acs.chemrev.9b00264
Chem. Rev. XXXX, XXX, XXX−XXX

(147) Baker, J. L.; Voth, G. A. Effects of ATP and Actin-Filament Binding on the Dynamics of the Myosin II S1 Domain. *Biophys. J.* **2013**, *105*, 1624−1634.
(148) Coates, J.; Criddle, A.; Geeves, M. Pressure-Relaxation Studies of Pyrene-Labelled Actin and Myosin Subfragment 1 from Rabbit Skeletal Muscle. Evidence for Two States of Acto-Subfragment 1. *Biochem. J.* **1985**, *232*, 351−356.
(149) Kim, E.; Bobkova, E.; Hegyi, G.; Muhlrad, A.; Reisler, E. Actin Cross-Linking and Inhibition of the Actomyosin Motor. *Biochemistry* **2002**, *41*, 86−93.
(150) Zimmermann, D.; Santos, A.; Kovar, D. R.; Rock, R. S. Actin Age Orchestrates Myosin-5 and Myosin-6 Run Lengths. *Curr. Biol.* **2015**, *25*, 2057−2062.
(151) Isambert, H.; Venier, P.; Maggs, A.; Fattoum, A.; Kassab, R.; Pantaloni, D.; Carlier, M. Flexibility of Actin Filaments Derived from Thermal Fluctuations. Effect of Bound Nucleotide, Phalloidin, and Muscle Regulatory Proteins. *J. Biol. Chem.* **1995**, *270*, 11437−11444.
(152) Korn, E.; Carlier, M.; Pantaloni, D. Actin Polymerization and ATP Hydrolysis. *Science* **1987**, *238*, 638−644.
(153) Tang, N.; Ostap, E. M. Motor Domain-Dependent Localization of Myo1b (Myr-1). *Curr. Biol.* **2001**, *11*, 1131−1135.
(154) Lieto-Trivedi, A.; Dash, S.; Coluccio, L. M. Myosin Surface Loop 4 Modulates Inhibition of Actomyosin 1b ATPase Activity by Tropomyosin. *Biochemistry* **2007**, *46*, 2779−2786.
(155) Furch, M.; Geeves, M. A.; Manstein, D. J. Modulation of Actin Affinity and Actomyosin Adenosine Triphosphatase by Charge Changes in the Myosin Motor Domain. *Biochemistry* **1998**, *37*, 6317−6326.
(156) Furch, M.; Remmel, B.; Geeves, M. A.; Manstein, D. J. Stabilization of the Actomyosin Complex by Negative Charges on Myosin. *Biochemistry* **2000**, *39*, 11602−11608.
(157) Lauzon, A.-M.; Tyska, M. J.; Rovner, A. S.; Freyzon, Y.; Warshaw, D. M.; Trybus, K. M. A 7-Amino-Acid Insert in the Heavy Chain Nucleotide Binding Loop Alters the Kinetics of Smooth Muscle Myosin in the Laser Trap. *J. Muscle Res. Cell Motil.* **1998**, *19*, 825−837.
(158) Kurzawa-Goertz, S.; Perreault-Micale, C.; Trybus, K.; Szent-Györgyi, A.; Geeves, M. Loop I Can Modulate ADP Affinity, ATPase Activity, and Motility of Different Scallop Myosins. Transient Kinetic Analysis of S1 Isoforms. *Biochemistry* **1998**, *37*, 7517−7525.
(159) Greenberg, M. J.; Lin, T.; Shuman, H.; Ostap, M. E. Mechanochemical Tuning of Myosin-I by the N-Terminal Region. *Proc. Natl. Acad. Sci. U. S. A.* **2015**, *112*, E3337−E3344.
(160) Lehman, W.; Orzechowski, M.; Li, X.; Fischer, S.; Raunser, S. Gestalt-Binding of Tropomyosin on Actin during Thin Filament Activation. *J. Muscle Res. Cell Motil.* **2013**, *34*, 155−163.
(161) Risi, C.; Eisner, J.; Belknap, B.; Heeley, D. H.; White, H. D.; Schröder, G. F.; Galkin, V. E. Ca2+-Induced Movement of Tropomyosin on Native Cardiac Thin Filaments Revealed by Cryoelectron Microscopy. *Proc. Natl. Acad. Sci. U. S. A.* **2017**, *114*, 6782−6787.
(162) Joel, P. B.; Trybus, K. M.; Sweeney, H. L. Two Conserved Lysines at the 50/20-KDa Junction of Myosin Are Necessary for Triggering Actin Activation. *J. Biol. Chem.* **2001**, *276*, 2998−3003.
(163) Várkuti, B. H.; Yang, Z.; Kintses, B.; Erdélyi, P.; Bárdos-Nagy, I.; Kovács, A. L.; Hári, P.; Kellermayer, M.; Vellai, T.; Málnási-Csizmadia, A. A Novel Actin Binding Site of Myosin Required for Effective Muscle Contraction. *Nat. Struct. Mol. Biol.* **2012**, *19*, 299−306.
(164) Yanagida, T.; Arata, T.; Oosawa, F. Sliding Distance of Actin Filament Induced by a Myosin Crossbridge during One ATP Hydrolysis Cycle. *Nature* **1985**, *316*, 366−369.
(165) Veigel, C.; Wang, F.; Bartoo, M. L.; Sellers, J. R.; Molloy, J. E. The Gated Gait of the Processive Molecular Motor. *Nat. Cell Biol.* **2002**, *4*, 59−65.
(166) Caremani, M.; Dantzig, J.; Goldman, Y. E.; Lombardi, V.; Linari, M. Effect of Inorganic Phosphate on the Force and Number of Myosin Cross-Bridges During the Isometric Contraction of Permeabilized Muscle Fibers from Rabbit Psoas. *Biophys. J.* **2008**, *95*, 5798−5808.
(167) Takagi, Y.; Homsher, E. E.; Goldman, Y. E.; Shuman, H. Force Generation in Single Conventional Actomyosin Complexes under High Dynamic Load. *Biophys. J.* **2006**, *90*, 1295−1307.
(168) Sellers, J. R.; Veigel, C. Direct Observation of the Myosin-Va Power Stroke and Its Reversal. *Nat. Struct. Mol. Biol.* **2010**, *17*, 590−595.
(169) Woody, M.; Winkelmann, D.; Capitanio, M.; Ostap, M. E.; Goldman, Y. E. Single Molecule Mechanics Resolves the Earliest Events in Force Generation by Cardiac Myosin. *eLife* **2019**, *8*, No. e49266.
(170) Preller, M.; Holmes, K. C. The Myosin Start-of-power Stroke State and How Actin Binding Drives the Power Stroke. *Cytoskeleton* **2013**, *70*, 651−660.
(171) Houdusse, A.; Sweeney, H. L. Myosin Motors: Missing Structures and Hidden Springs. *Curr. Opin. Struct. Biol.* **2001**, *11*, 182−194.
(172) Kiani, F.; Fischer, S. ATP-dependent Interplay between Local and Global Conformational Changes in the Myosin Motor. *Cytoskeleton* **2016**, *73*, 643−651.
(173) Onishi, H.; Mikhailenko, S. V.; Morales, M. F. Toward Understanding Actin Activation of Myosin ATPase: The Role of Myosin Surface Loops. *Proc. Natl. Acad. Sci. U. S. A.* **2006**, *103*, 6136−6141.
(174) Stehle, R. Force Responses and Sarcomere Dynamics of Cardiac Myofibrils Induced by Rapid Changes in [Pi]. *Biophys. J.* **2017**, *112*, 356−367.
(175) Stehle, R.; Tesi, C. Kinetic Coupling of Phosphate Release, Force Generation and Rate-Limiting Steps in the Cross-Bridge Cycle. *J. Muscle Res. Cell Motil.* **2017**, *38*, 275−289.
(176) Homsher, E. A New and Improved View of Force Production. *Biophys. J.* **2017**, *112*, 205−206.
(177) Muretta, J. M.; Rohde, J. A.; Johnsrud, D. O.; Cornea, S.; Thomas, D. D. Direct Real-Time Detection of the Structural and Biochemical Events in the Myosin Power Stroke. *Proc. Natl. Acad. Sci. U. S. A.* **2015**, *112*, 14272−14277.
(178) Trivedi, D. V.; Muretta, J. M.; Swenson, A. M.; Davis, J. P.; Thomas, D. D.; Yengo, C. M. Direct Measurements of the Coordination of Lever Arm Swing and the Catalytic Cycle in Myosin V. *Proc. Natl. Acad. Sci. U. S. A.* **2015**, *112*, 14593−14598.
(179) Dantzig, J.; Goldman, Y.; Millar, N.; Lacktis, J.; Homsher, E. Reversal of the Cross-bridge Force-generating Transition by Photogeneration of Phosphate in Rabbit Psoas Muscle Fibres. *J. Physiol.* **1992**, *451*, 247−278.
(180) Coupling between Phosphate Release and Force Generation in Muscle Actomyosin. *Philos. Trans. R. Soc., B* **2004**, *359*, 1913−1920.
(181) Linari, M.; Caremani, M.; Lombardi, V. A Kinetic Model That Explains the Effect of Inorganic Phosphate on the Mechanics and Energetics of Isometric Contraction of Fast Skeletal Muscle. *Proc. R. Soc. London, Ser. B* **2010**, *277*, 19−27.
(182) Rüegg, J.; Schädler, M.; Steiger, G.; Müller, G. Effects of Inorganic Phosphate on the Contractile Mechanism. *Pfluegers Arch.* **1971**, *325*, 359−364.
(183) Cooke, R.; Pate, E. The Effects of ADP and Phosphate on the Contraction of Muscle Fibers. *Biophys. J.* **1985**, *48*, 789−798.
(184) Cecchini, M.; Houdusse, A.; Karplus, M. Allosteric Communication in Myosin V: From Small Conformational Changes to Large Directed Movements. *PLoS Comput. Biol.* **2008**, *4*, No. e1000129.
(185) Rohde, J. A.; Thomas, D. D.; Muretta, J. M. Heart Failure Drug Changes the Mechanoenzymology of the Cardiac Myosin Powerstroke. *Proc. Natl. Acad. Sci. U. S. A.* **2017**, *114*, E1796−E1804.
(186) Woody, M. S.; Greenberg, M. J.; Barua, B.; Winkelmann, D. A.; Goldman, Y. E.; Ostap, M. E. Positive Cardiac Inotrope Omecamtiv Mecarbil Activates Muscle despite Suppressing the Myosin Working Stroke. *Nat. Commun.* **2018**, *9*, 3838.

DOI: 10.1021/acs.chemrev.9b00264
Chem. Rev. XXXX, XXX, XXX−XXX

(187) Fenn, W. O. A Quantitative Comparison between the Energy Liberated and the Work Performed by the Isolated Sartorius Muscle of the Frog. *J. Physiol.* **1923**, *58*, 175−203.
(188) Fenn, W. O. The Relation between the Work Performed and the Energy Liberated in Muscular Contraction. *J. Physiol.* **1924**, *58*, 373−395.
(189) Veigel, C.; Molloy, J. E.; Schmitz, S.; Kendrick-Jones, J. Load-Dependent Kinetics of Force Production by Smooth Muscle Myosin Measured with Optical Tweezers. *Nat. Cell Biol.* **2003**, *5*, 980−986.
(190) Iwaki, M.; Wickham, S.; Ikezaki, K.; Yanagida, T.; Shih, W. A Programmable DNA Origami Nanospring That Reveals Force-Induced Adjacent Binding of Myosin VI Heads. *Nat. Commun.* **2016**, *7*, 13715.
(191) Ikezaki, K.; Komori, T.; Sugawa, M.; Arai, Y.; Nishikawa, S.; Iwane, A. H.; Yanagida, T. Simultaneous Observation of the Lever Arm and Head Explains Myosin VI Dual Function. *Small* **2012**, *8*, 3035−3040.
(192) Colombini, B.; Nocella, M.; Benelli, G.; Cecchi, G.; Griffiths, P. J.; Bagni, A. M. Reversal of the Myosin Power Stroke Induced by Fast Stretching of Intact Skeletal Muscle Fibers. *Biophys. J.* **2009**, *97*, 2922−2929.
(193) Walker, M. L.; Burgess, S. A.; Sellers, J. R.; Wang, F.; Hammer, J. A.; Trinick, J.; Knight, P. J. Two-Headed Binding of a Processive Myosin to F-Actin. *Nature* **2000**, *405*, 804−807.
(194) Oke, O. A.; Burgess, S. A.; Forgacs, E.; Knight, P. J.; Sakamoto, T.; Sellers, J. R.; White, H.; Trinick, J. Influence of Lever Structure on Myosin 5a Walking. *Proc. Natl. Acad. Sci. U. S. A.* **2010**, *107*, 2509−2514.
(195) Uchihashi, T.; Kodera, N.; Ando, T. Guide to Video Recording of Structure Dynamics and Dynamic Processes of Proteins by High-Speed Atomic Force Microscopy. *Nat. Protoc.* **2012**, *7*, 1193−1206.
(196) Kodera, N.; Ando, T. The Path to Visualization of Walking Myosin V by High-Speed Atomic Force Microscopy. *Biophys. Rev.* **2014**, *6*, 237−260.
(197) Rosenfeld, S. S.; Sweeney, H. L. A Model of Myosin V Processivity. *J. Biol. Chem.* **2004**, *279*, 40100−40111.
(198) Liu, C.; Kawana, M.; Song, D.; Ruppel, K. M.; Spudich, J. A. Controlling Load-Dependent Kinetics of β-Cardiac Myosin at the Single-Molecule Level. *Nat. Struct. Mol. Biol.* **2018**, *25*, 505−514.

DOI: 10.1021/acs.chemrev.9b00264
Chem. Rev. XXXX, XXX, XXX−XXX